

Large-Scale Fluid-Structure Interaction Simulation of Viscoplastic and Fracturing Thin- Shells Subjected to Shocks and Detonations

Fehmi Cirak
University of Cambridge, UK

Ralf Deiterding
Oak Ridge National Laboratory

Sean P. Mauch
California Institute of Technology

4th Fourth M.I.T. Conference on Computational Fluid and Solid Mechanics
June 13, 2007

This work is sponsored by the Office of Advanced Scientific Computing Research; U.S. Department of Energy (DOE) and was performed at the Oak Ridge National Laboratory, which is managed by UT-Battelle, LLC under Contract No. DE-AC05-00OR22725. Part of this work was also performed at the California Institute of Technology and was supported by the ASC program of the Department of Energy under subcontract No. B341492 of DOE contract W-7405-ENG-48.

Outline of the talk

- Eulerian fluid solver
 - *Governing equations*
 - *Level-set-based ghost fluid approach*
 - *Structured adaptive mesh refinement*
 - *Verification and validation*
- Fluid-structure coupling
 - *Algorithmic approach*
 - *Level set evaluation*
- Thin-shell solid mechanics solver
 - *Modeling of fracture*
- Detonation-driven fracture of thin tubes
 - *Detonation model*
 - *Validation of fluid-structure coupling in elastic and plastic regime*
- Deformation of thin plates in a water shocktube
 - *Plastic deformation*
 - *Preliminary fracture results*
- Outlook on software, conclusions

Hydrodynamic equations

Euler equations

$$\frac{\partial \rho}{\partial t} + \frac{\partial}{\partial x_k}(\rho u_k) = 0$$

$$\frac{\partial}{\partial t}(\rho u_i) + \frac{\partial}{\partial x_k}(\rho u_i u_k + \delta_{ik} p) = 0$$

$$\frac{\partial E}{\partial t} + \frac{\partial}{\partial x_k}(u_k(E + p)) = 0$$

Stiffened gas equation of state

$$p = (\gamma - 1)(E - \frac{1}{2}u_k u_k) - \gamma p_\infty$$

Hydrodynamic equations

Euler equations with reaction

$$\frac{\partial \rho}{\partial t} + \frac{\partial}{\partial x_k}(\rho u_k) = 0$$

$$\frac{\partial}{\partial t}(\rho u_i) + \frac{\partial}{\partial x_k}(\rho u_i u_k + \delta_{ik} p) = 0$$

$$\frac{\partial E}{\partial t} + \frac{\partial}{\partial x_k}(u_k(E + p)) = 0$$

$$\frac{\partial}{\partial t}(\rho Y) + \frac{\partial}{\partial x_k}(\rho Y u_k) = W\dot{\omega}$$

Equation of state with heat release

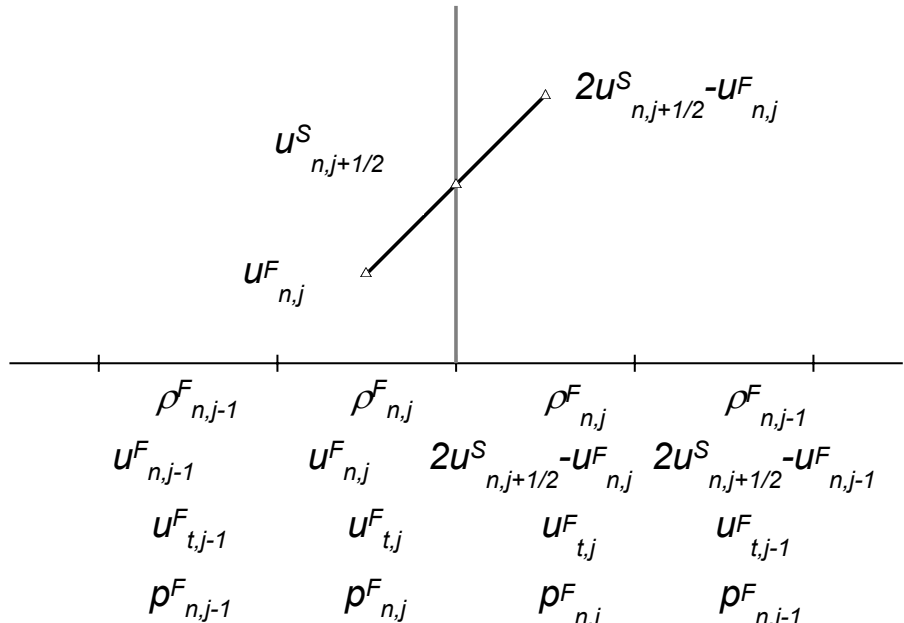
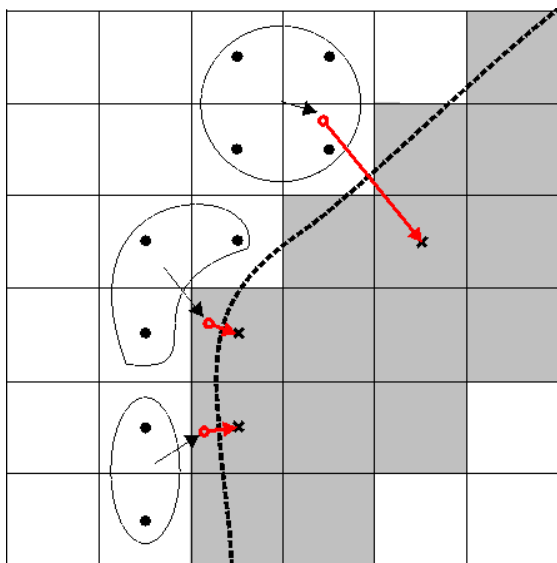
$$p = (\gamma - 1)(E - \frac{1}{2}\rho u_k u_k - \rho Y q)$$

Single exothermic chemical reaction

$$W\dot{\omega} = -A\rho \exp(-E/\mathcal{R}T)$$

Embedded boundary method

- Incorporate complex moving boundary/interfaces into a Cartesian solver (extension of work by R.Fedkiw and T.Aslam)
- Implicit boundary representation via distance function φ , normal $n = \nabla\varphi / |\nabla\varphi|$
- Treat an interface as a moving rigid wall
- Method diffuses boundary and is therefore not conservative
- Construction of values in embedded boundary cells by interpolation / extrapolation



$$\text{Velocity: } \mathbf{u}^F_{Gh} = 2((\mathbf{u}^S - \mathbf{u}^F_M) \cdot \mathbf{n}) \mathbf{n} + \mathbf{u}^F_M$$

- Higher resolution at embedded boundary required than with first-order unstructured scheme
- Appropriate level-set-based refinement criteria are available to cure deficiencies

Structured AMR for hyperbolic problems

- For simplicity

$$\partial_t q + \nabla \cdot f(q) = 0$$

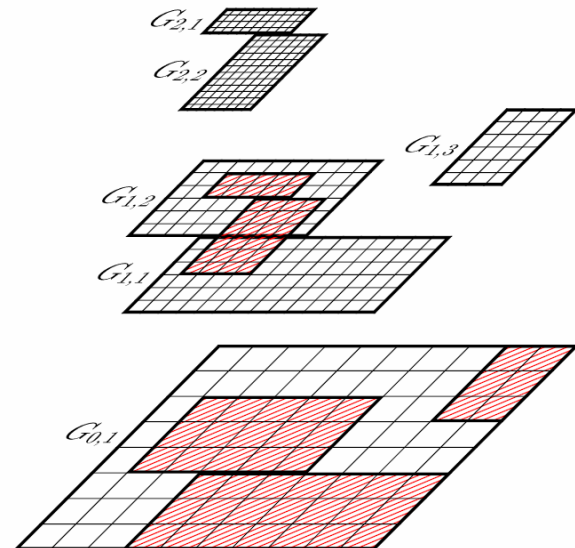
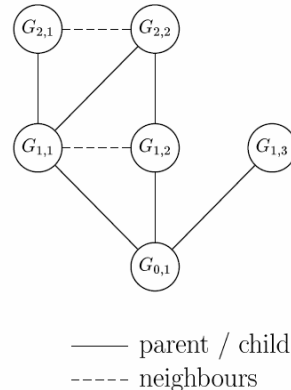
- Refined subgrids overlay coarser ones
- Computational decoupling of subgrids by using ghost cells
- Refinement in space *and* time
- Block-based data structures
- Cells without mark are refined
- Cluster-algorithm necessary
- Efficient cache-reuse / vectorization possible
- Explicit finite volume scheme

$$Q_{jk}^{n+1} = Q_{jk}^n - \frac{\Delta t}{\Delta x_1} [F_{j+\frac{1}{2},k}^1 - F_{j-\frac{1}{2},k}^1] - \frac{\Delta t}{\Delta x_2} [F_{j,k+\frac{1}{2}}^2 - F_{j,k-\frac{1}{2}}^2]$$

only for single rectangular grid necessary

- M. Berger and P. Colella, J. Comput. Phys. 82, 1988.

Grid hierarchy



Root Level

$$r_0 = 1$$

1

$$r_1 = 4$$

11

$$r_2 = 2$$

13

Time

Regridding of finer levels.
Base level () stays fixed.

Parallelization strategy

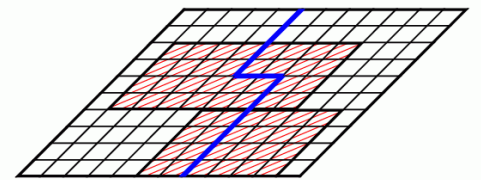
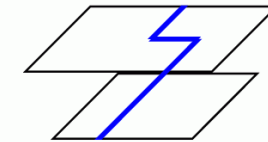
Domain decomposition: $G_0 = \bigcup_{p=1}^P G_0^p$ with $G_0^p \cap G_0^q = \emptyset$ for $p \neq q$

$$G_0^p := \bigcup_{m=1}^{M_0^p} G_{0,m}^p \quad \longrightarrow \quad G_l^p := G_l \cap G_0^p$$

Workload: $\mathcal{W}(\Omega) = \sum_{l=0}^{l_{\max}} \left[\mathcal{N}_l(G_l \cap \Omega) \prod_{\kappa=0}^l r_\kappa \right]$, $\mathcal{N}_l(G)$ No. of cells on l

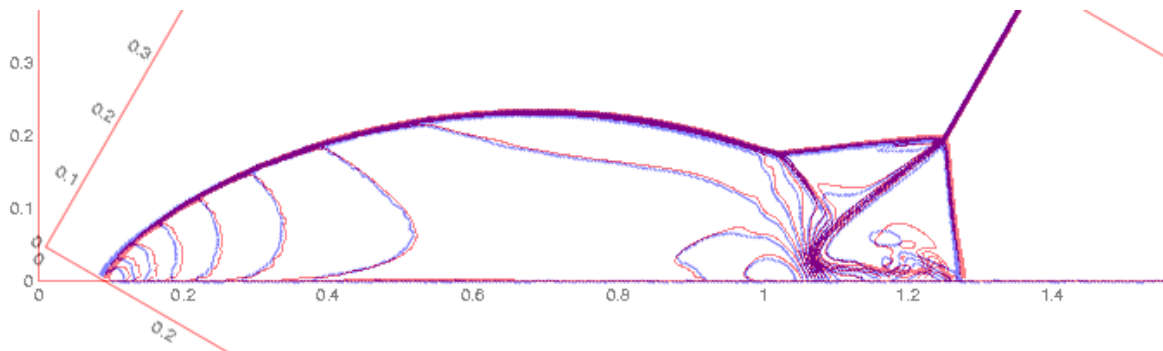
Load-balancing: $\mathcal{L}^p := \frac{P \cdot \mathcal{W}(G_0^p)}{\mathcal{W}(G_0)} \approx 1$ for all $p = 1, \dots, P$

Processor 1 Processor 2

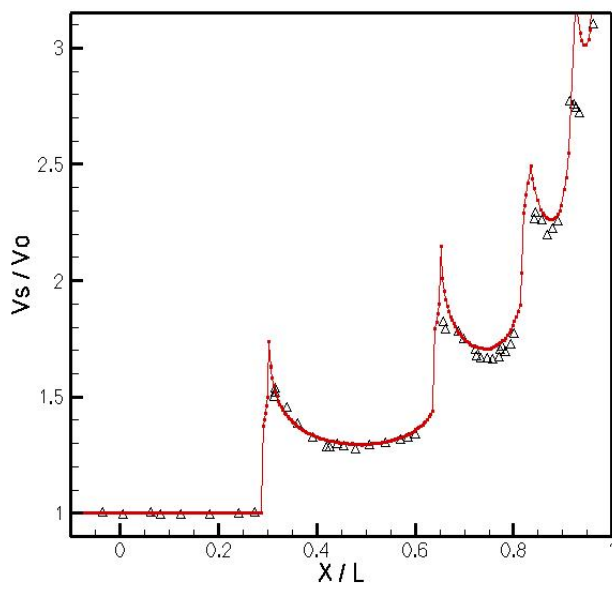


- Data of all levels resides on same node \rightarrow Interpolation and averaging remain strictly local
- Only parallel operations to be considered:
 - *Parallel synchronization as part of ghost cell setting*
 - *Load-balanced repartitioning of data blocks as part of `Regrid(1)`*
 - *Application of flux correction terms on coarse-grid cells*
- Partitioning at root level with generalized Hilbert space-filling curve by M. Parashar

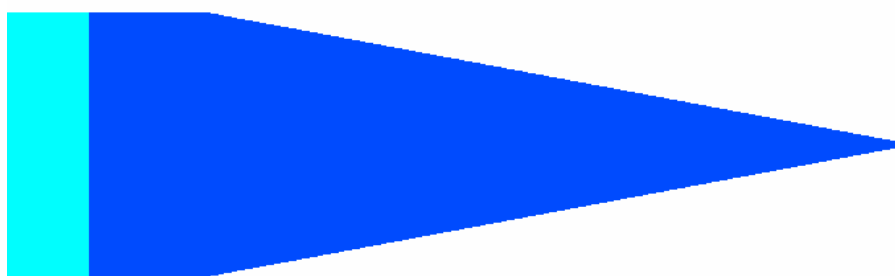
Verification of GFM



Double Mach reflection
Overlay of two simulation
of a double Mach
reflection on a 800x400
grid with GFM and 2nd
order accurate scheme



Conical shocktube
Cylindrical symmetric
simulation by D. Hill of
experiment by Setchel,
Strom and Sturtevant
(JFM 1972)
Mach 6 shock in Argon



Left: shock velocity along centerline in experiment and simulation (red)

Shock interaction at double-wedge geometry

- Simulation by D. Hill
- Mach 9 flow in air hitting a double-wedge (15° and 45°)
- Example from Olejniczak, Wright and Candler (JFM 1997)
- AMR base mesh 300×100 , 3 additional levels with factor 2
- 3rd order WENO computation vs. 2nd order MUSCL with van Leer flux vector splitting

10

J. Olejniczak, M. J. Wright and G. V. Candler

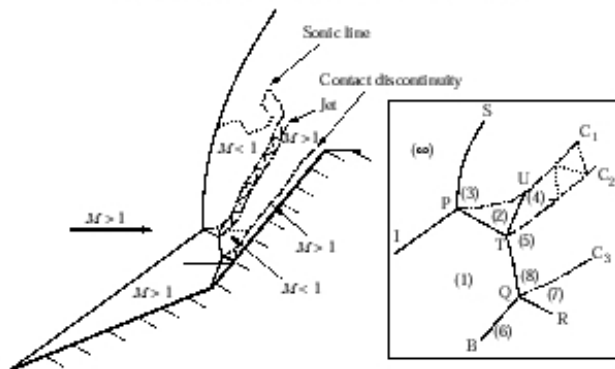
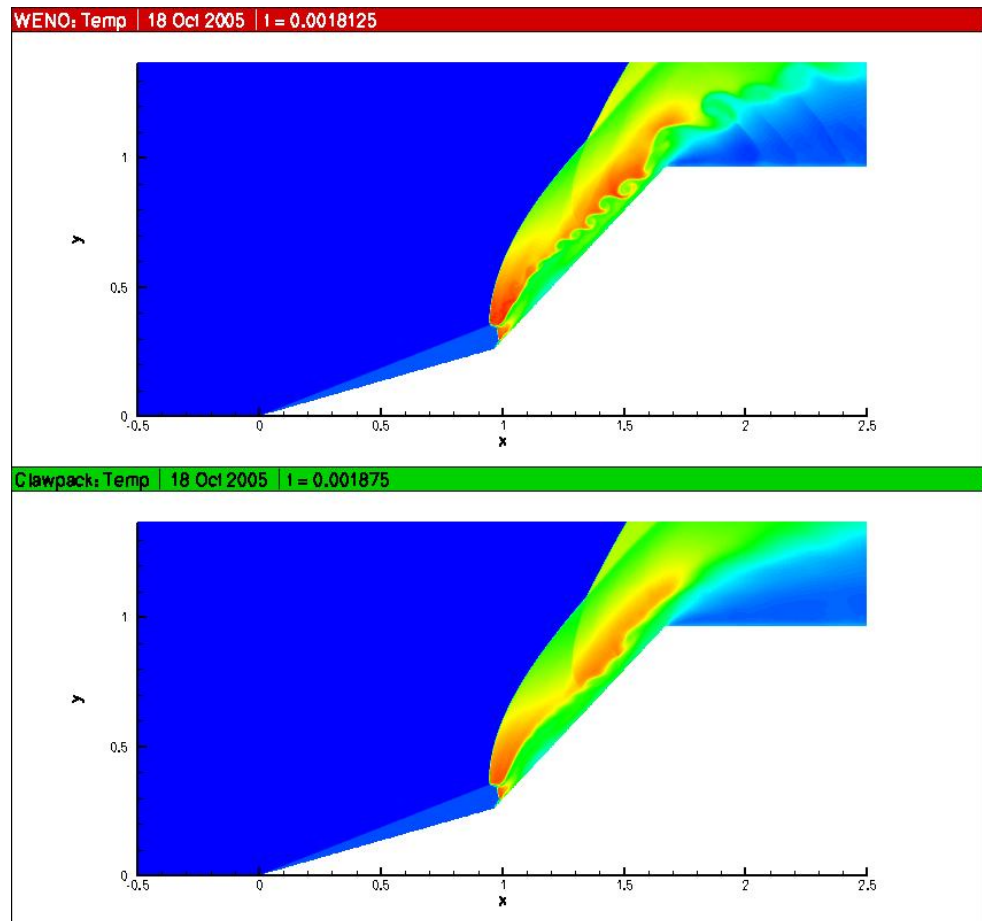
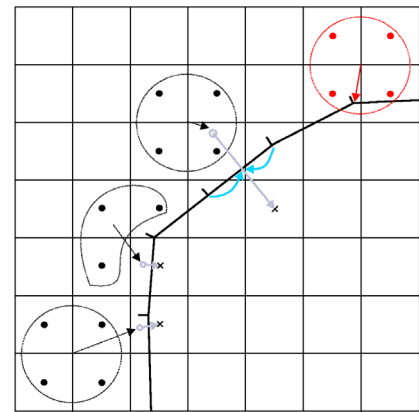


FIGURE 6. Schematic diagram of a Type V shock interaction with an enlargement of the interaction region.

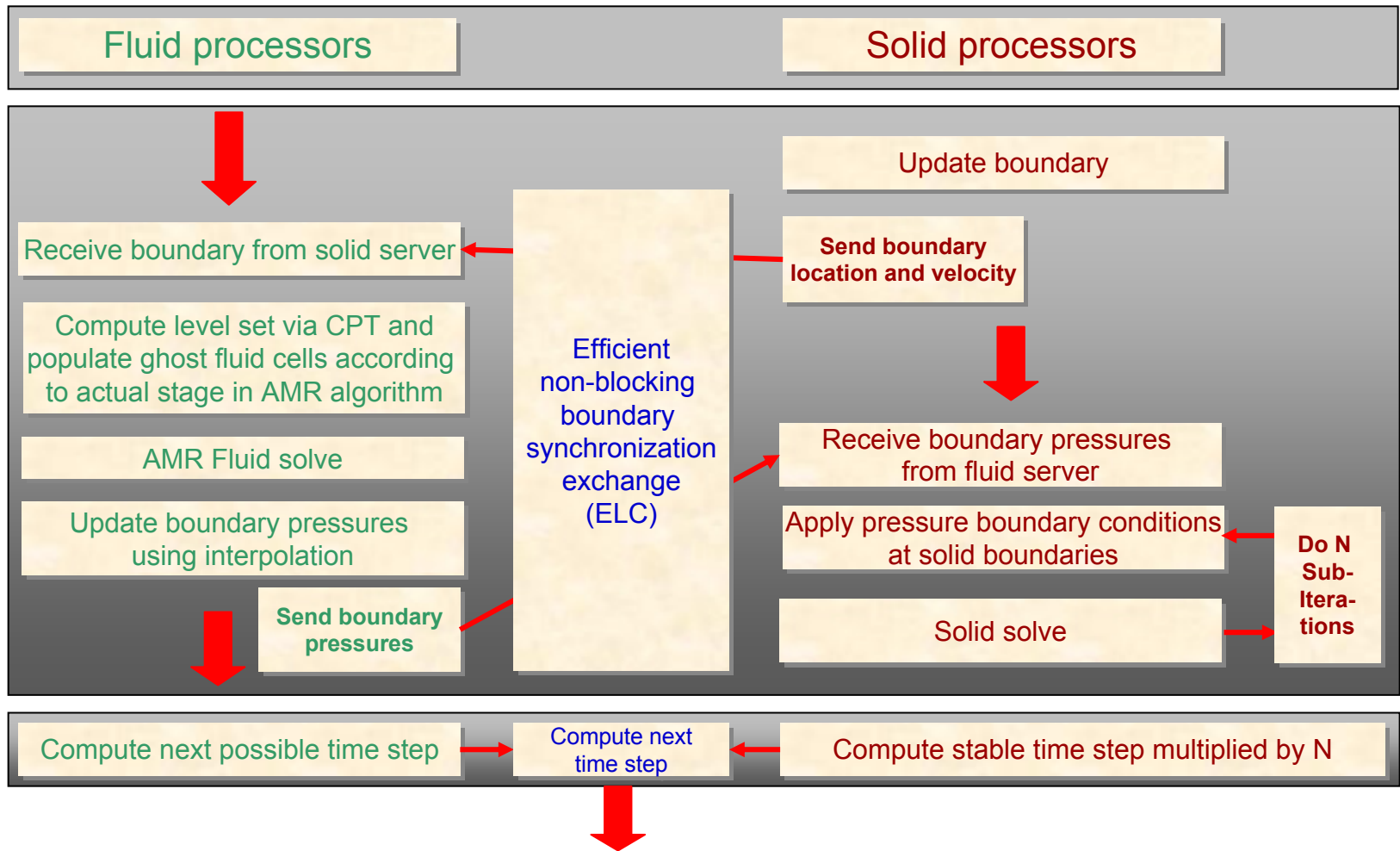


Fluid-structure coupling

- Couple compressible Euler equations to Lagrangian structure mechanics
- Compatibility conditions between inviscid fluid and solid at a slip interface
 - Continuity of normal velocity: $u^S_n = u^F_n$
 - Continuity of normal stresses: $\sigma_{nn}^S = -p^F$
 - No shear stresses: $\sigma_{n\tau}^S = \sigma_{n\omega}^S = 0$
- Time-splitting approach for coupling
 - *Fluid:*
 - Treat evolving solid surface with moving wall boundary conditions in fluid
 - Use solid surface mesh to calculate fluid level set
 - Use nearest velocity values u^S on surface facets to impose u^F_n in fluid
 - *Solid:*
 - Use interpolated hydro-pressure p^F to prescribe σ_{nn}^S on boundary facets
- Ad-hoc separation in dedicated fluid and solid processors

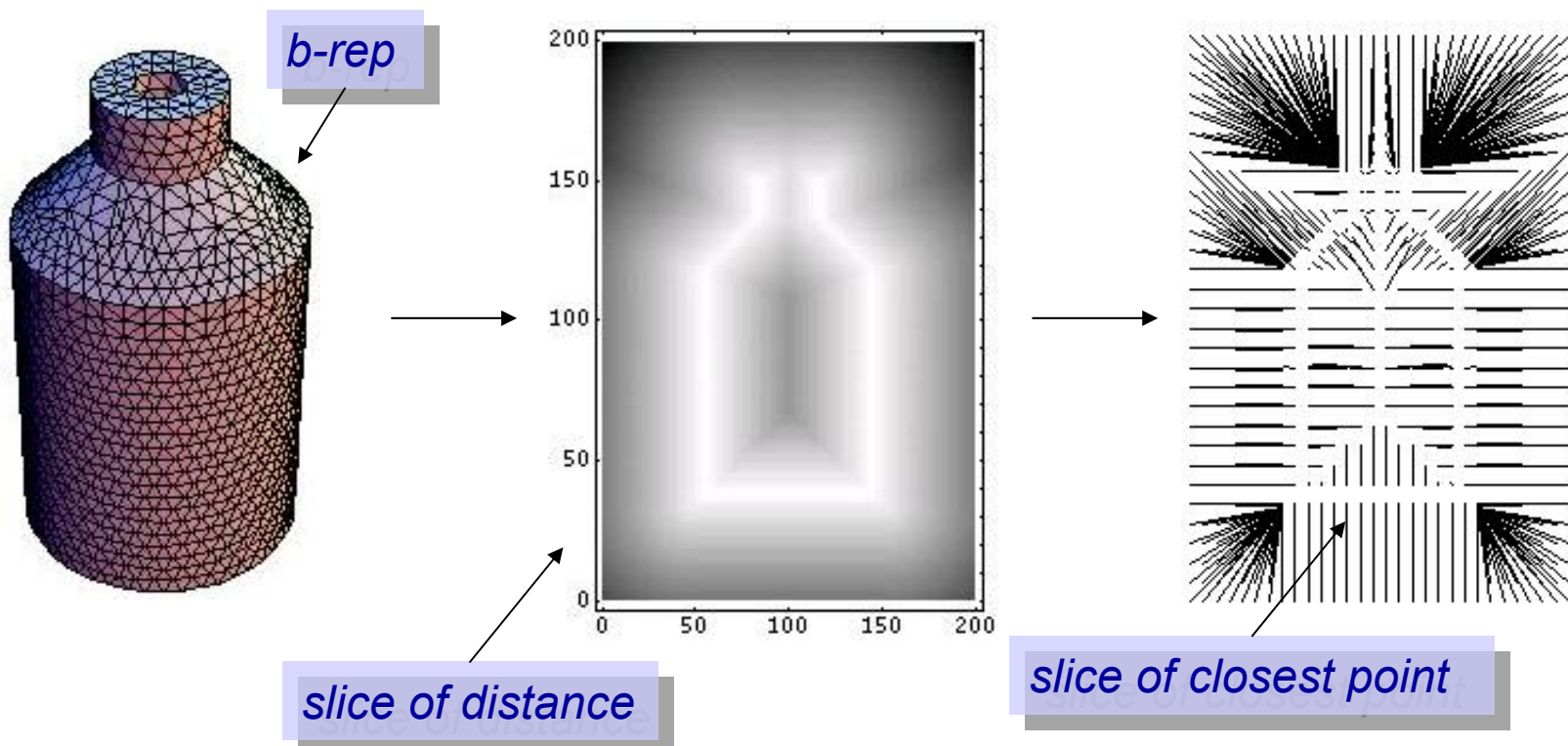


Algorithmic approach for coupling



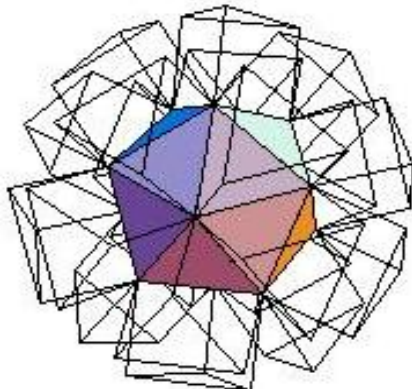
Implicit representations of complex surfaces

- FEM Solid Solver
 - *Explicit representation of the solid boundary, b-rep*
 - *Triangular faceted surface*
- Cartesian FV Solver
 - *Implicit level set representation*
 - *need closest point on the surface at each grid point*

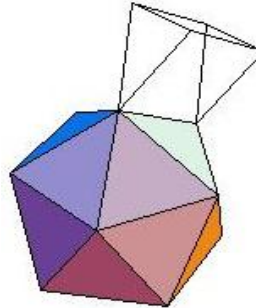


CPT in linear time

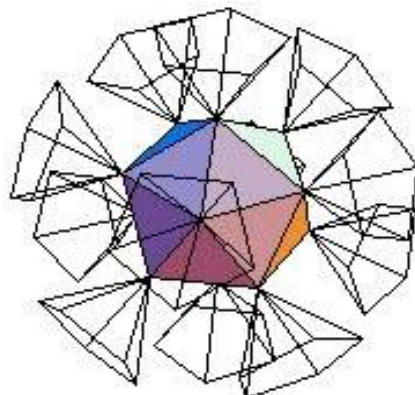
- Problem reduction by evaluation only within specified max. distance
- The characteristic / scan conversion algorithm.
 - *For each face/edge/vertex.*
 - *Scan convert the polyhedron.*
 - *Find distance, closest point to that primitive for the scan converted points.*
- Computational complexity.
 - $O(m)$ to build the b-rep and the polyhedra.
 - $O(n)$ to scan convert the polyhedra and compute the distance, etc.



Face Polyhedra



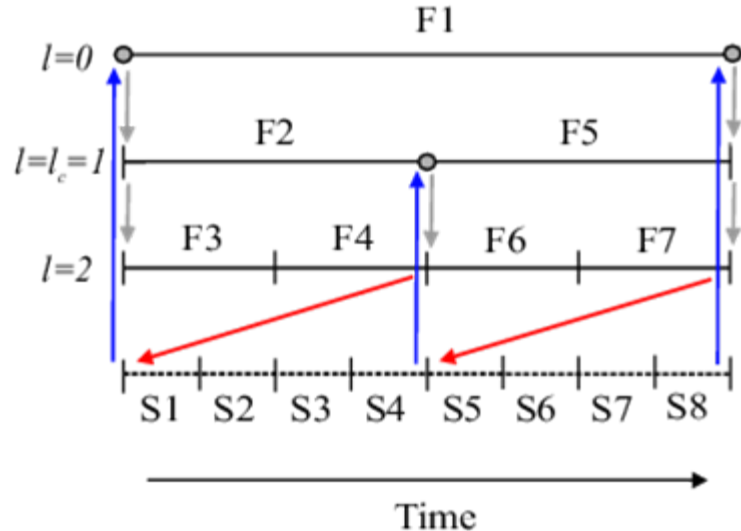
Edge Polyhedra



Vertex Polyhedra

Incorporation into hierarchical SAMR

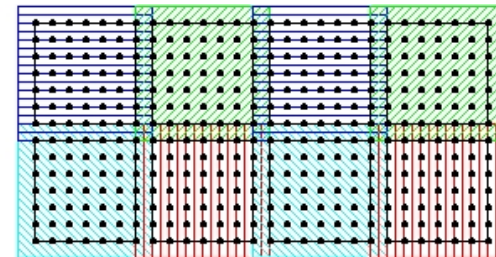
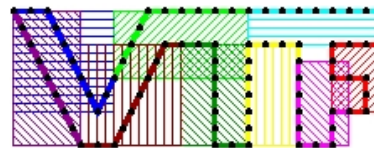
- Eulerian SAMR + non-adaptive Lagrangian FEM scheme
- Exploit SAMR time step refinement for effective coupling to solid solver
 - *Lagrangian simulation is called only at level $I_c < I_{max}$*
 - *SAMR refines solid boundary at least at level I_c*
 - *One additional level reserved to resolve ambiguities in GFM (e.g. thin structures)*
- Nevertheless: Inserting sub-steps accommodates for time step reduction from the solid solver within an SAMR cycle
- Communication strategy
 - *Updated boundary info from solid solver must be received (blue arrow) before regridding operation (gray dots and arrows)*
 - *Boundary data is sent to solid (red arrow) when highest level available*
- Inter-solver communication (point-to-point or globally) managed on the fly by current SAMR partition bounding box information by Eulerian-Lagrangian-Coupling module (ELC)



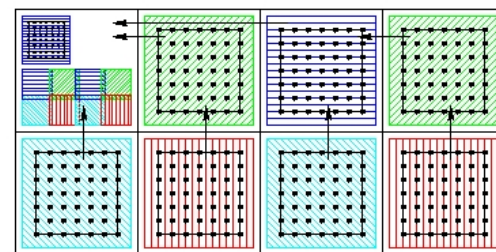
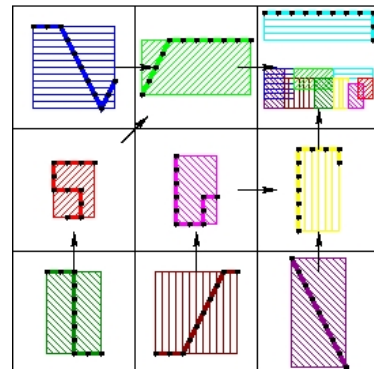
- *When SAMR mesh partitioning is done at runtime, the entire solid mesh must have been received (SAMR partitions must be allowed to change arbitrary)*
- *During strictly local regridding operations only the local portion of the solid mesh has to be received*

ELC communication module

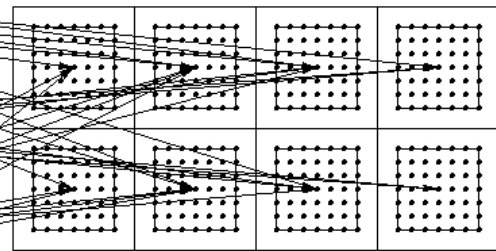
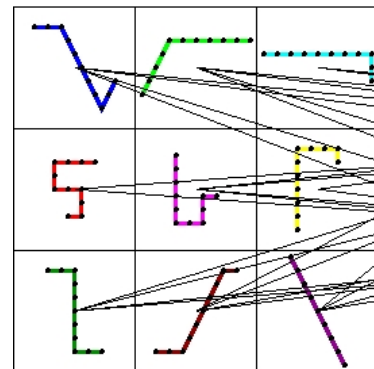
1. Put bounding boxes around each solid processor's piece of the boundary and around each fluid processor's grid.



2. Gather, exchange and broadcast of bounding box information

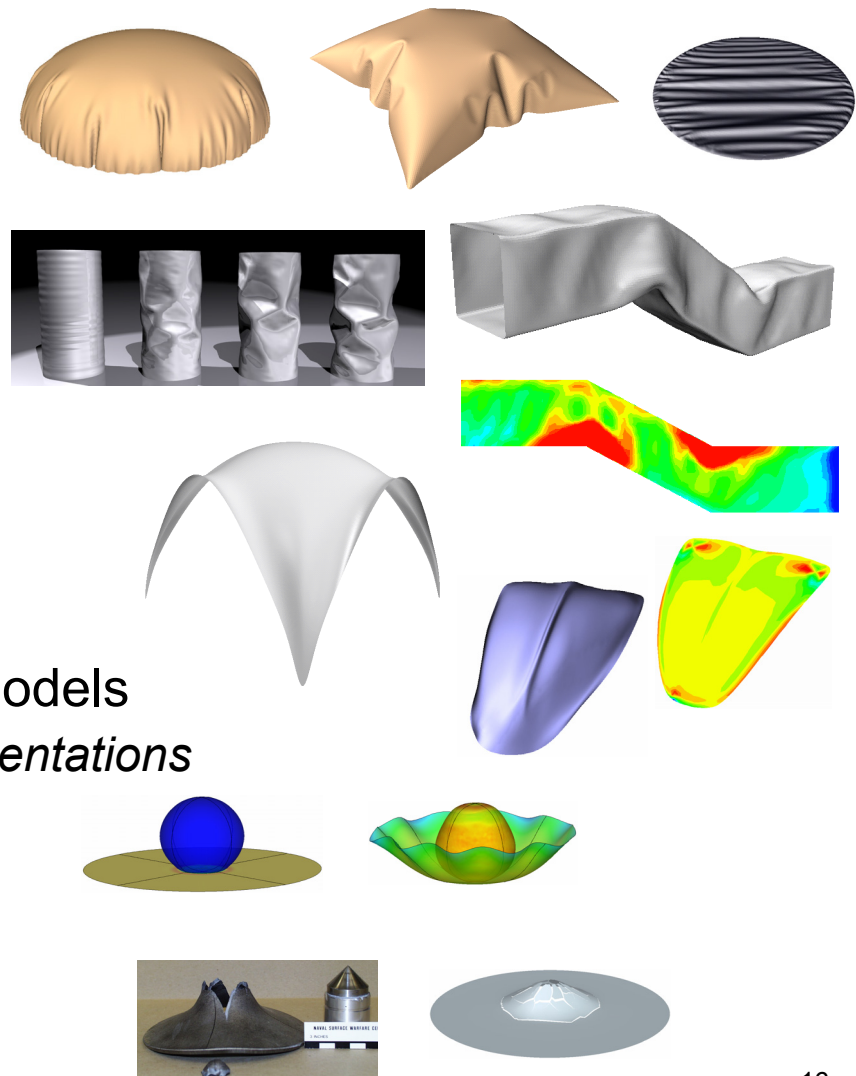


3. Optimal point-to-point communication pattern, non-blocking



Thin-shell finite element solver

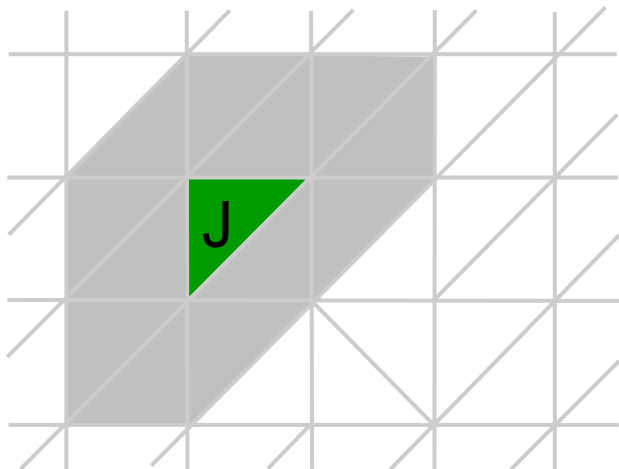
- Kirchhoff-Love shell theory
- Subdivision shell finite elements
 - *Stretching and bending resistance*
 - *Large deformations*
- Parallel explicit shell dynamics
 - *Fully scalable communications*
- Geometric modeling capabilities
- Access to a number of constitutive models
 - *Adlib models as well as own implementations*
- Parallel contact
- Fracture and fragmentation



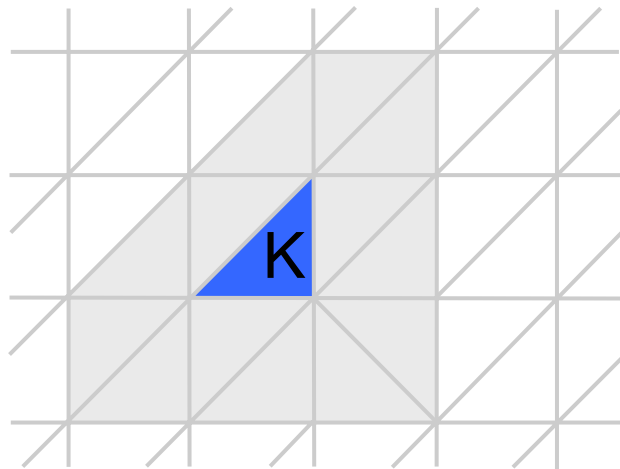
Subdivision FE Discretization

- Away from crack flanks, conforming FE discretization requires smooth shape functions
 - On regular patches, quartic box-splines are used
 - On irregular patches, subdivision schemes are used (here Loop's scheme)

Patch for element J



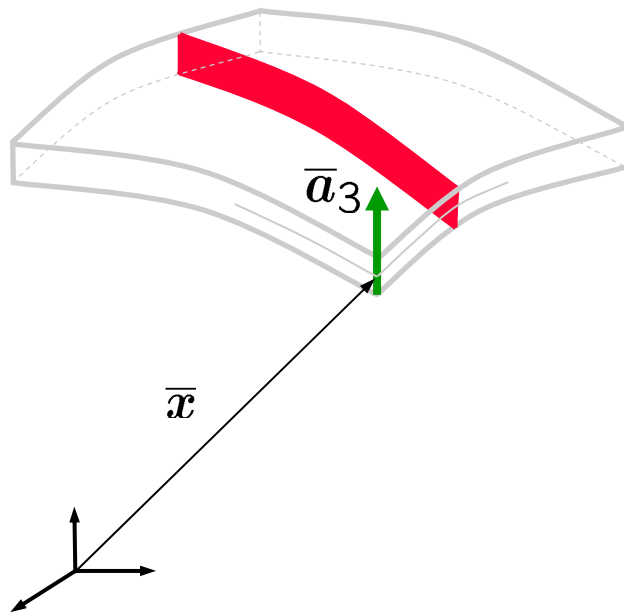
Patch for element K



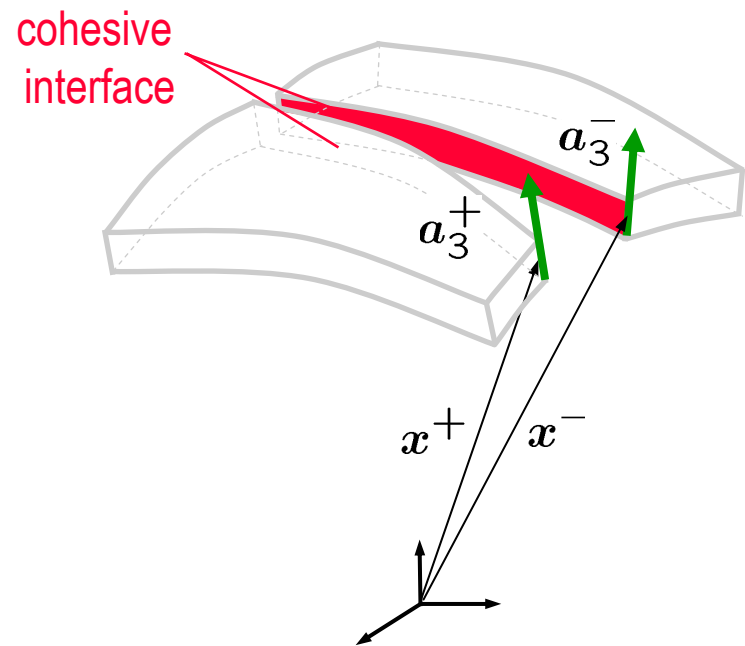
F. Cirak, M. Ortiz, P. Schröder, Int. J. Numer. Meth. Engrg. 47 (2000)

Fractured Thin-Shell Kinematics

Reference configuration



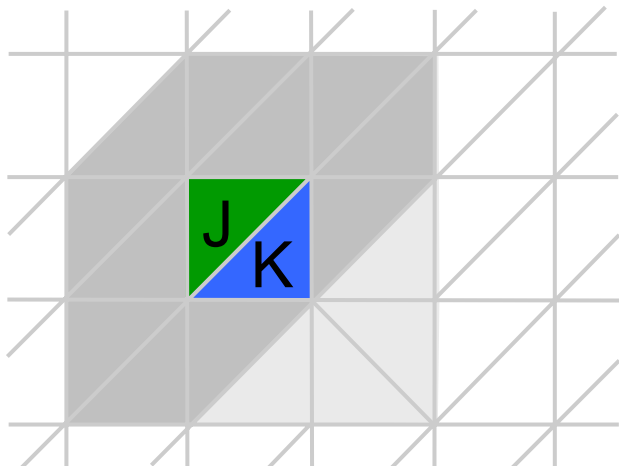
Deformed configuration



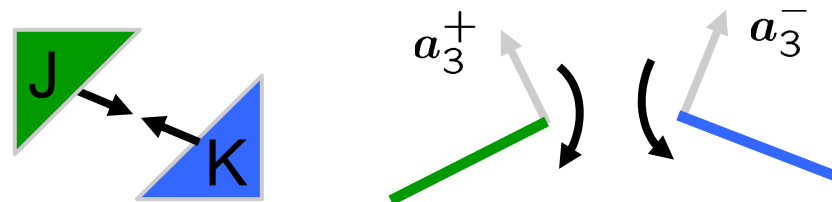
- Thin-shell assumption:
Spatial position of the fractured shell body is described by the middle surface position

Thin-Shell Fracture

- Each element is considered separately and cohesive interfaces are introduced on all edges



Interface deformations



Cohesive law



F. Cirak, M. Ortiz, A. Pandolfi, CMAME (2005)

FSI example: shock-induced panel motion

- Elastic motion of a thin steel plate (thickness $h=1\text{mm}$, length 50mm) hit by a Mach 1.21 shock wave in air, Giordano et al. Shock Waves (2005)
- Steel plate modeled with finite difference solver using the beam equation

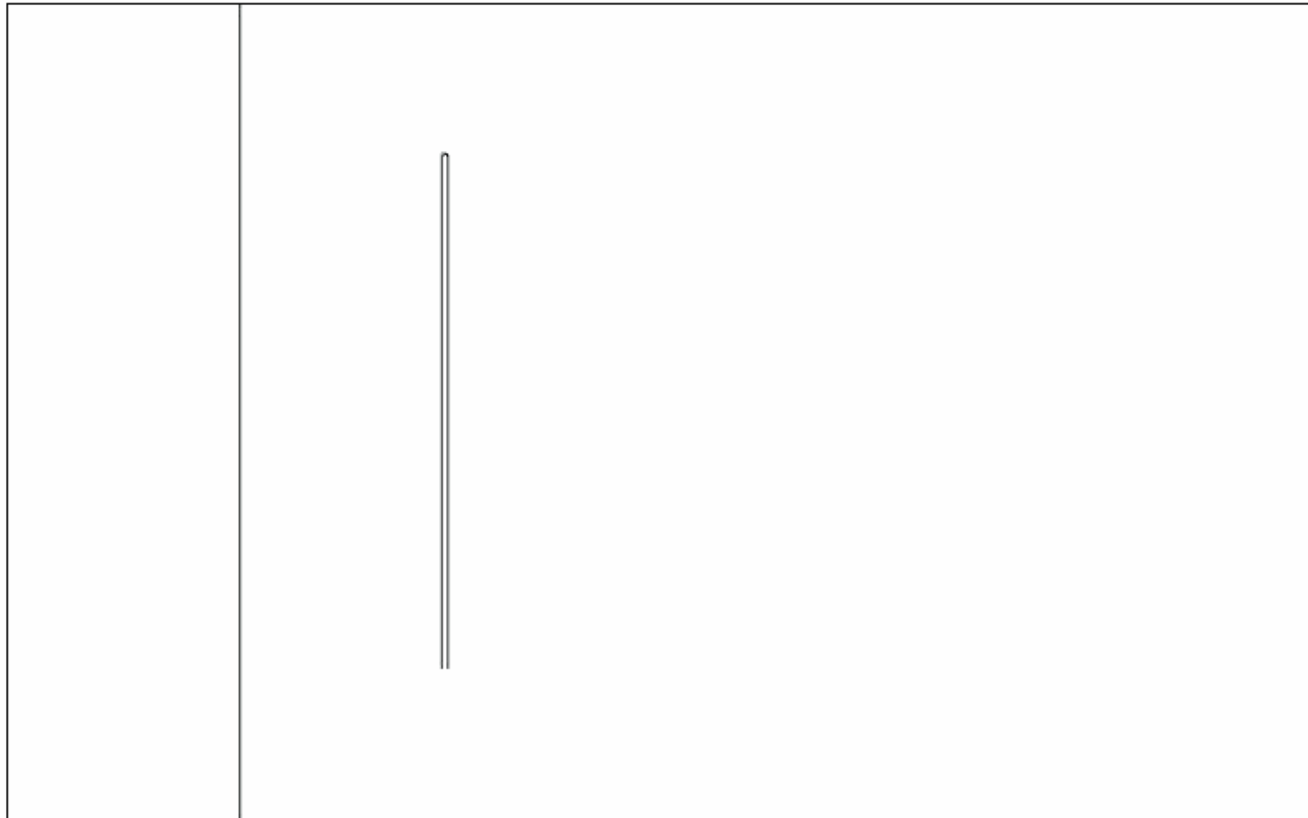
$$\rho h \frac{\partial^2 w}{\partial t^2} + EI \frac{\partial^4 w}{\partial x^4} = p(x, t)$$

- Forward facing step geometry, reflective boundaries everywhere except inflow at left side, panel 1.5cm behind start of step
- SAMR base mesh 320×64 , 2 additional level with factors 2, 4



Schlieren plot
of density

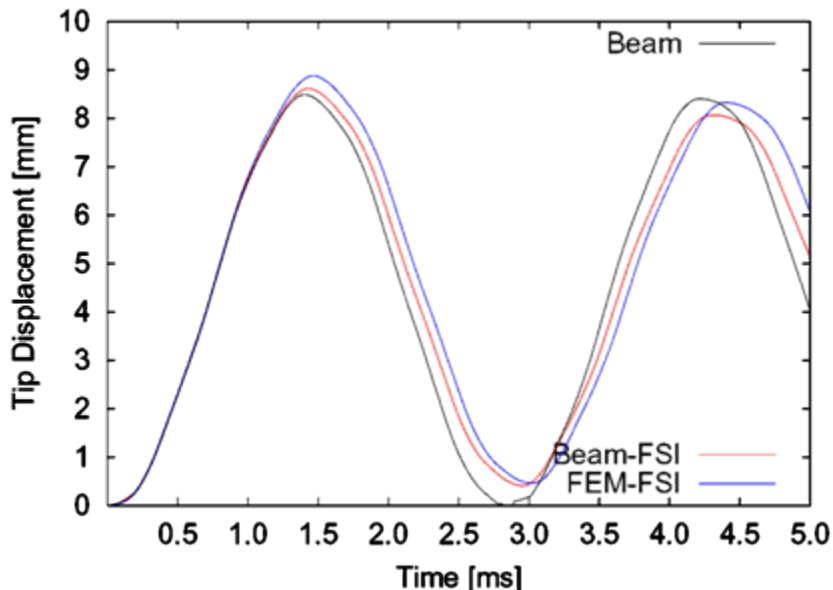
Shock-induced panel motion



Schlieren plot of density enlarged to
show panel motion

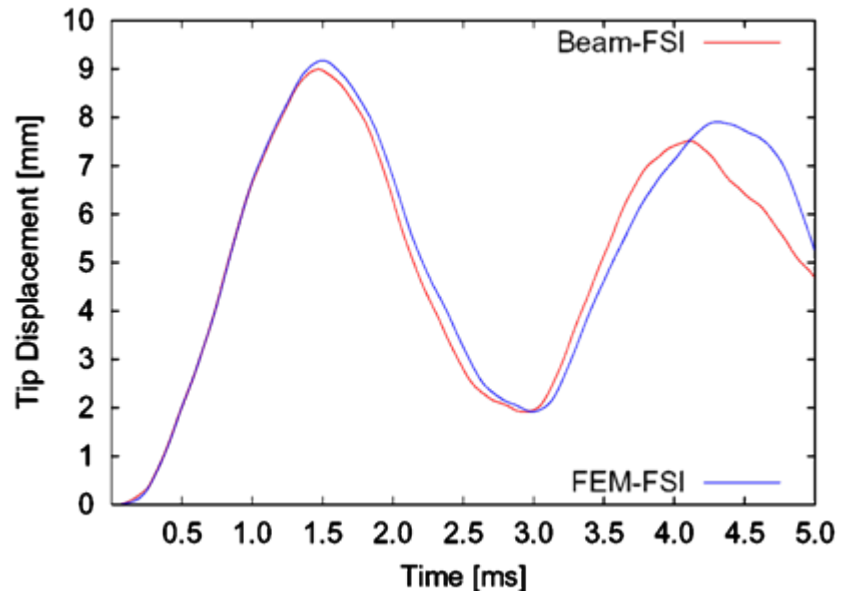
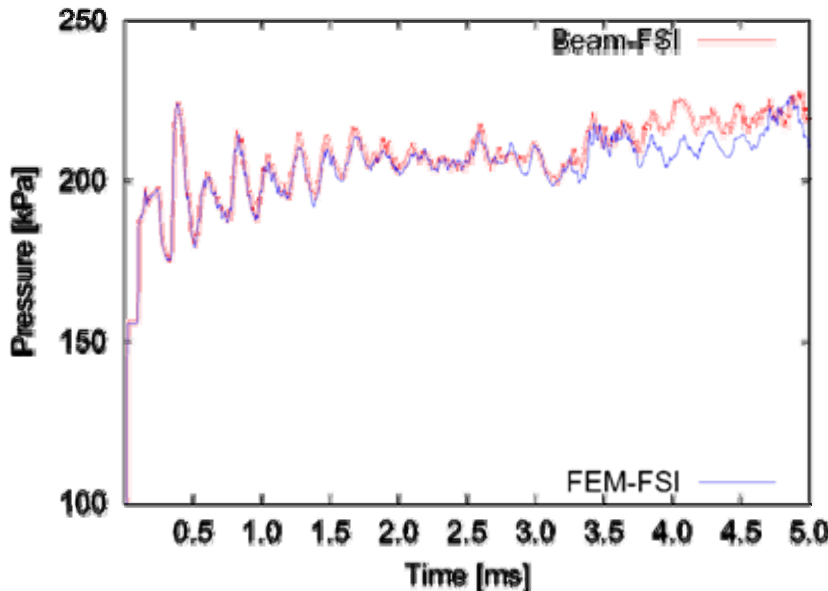
Panel motion – FSI verification

- FSI verification: constant impulsive loading of $\Delta p=100\text{kPa}$
 - Beam: No FSI
 - Beam-FSI: beam solver with coupled FV code
 - FEM-FSI: large displacement thin-shell finite element solver by F.Cirak coupled to FV code



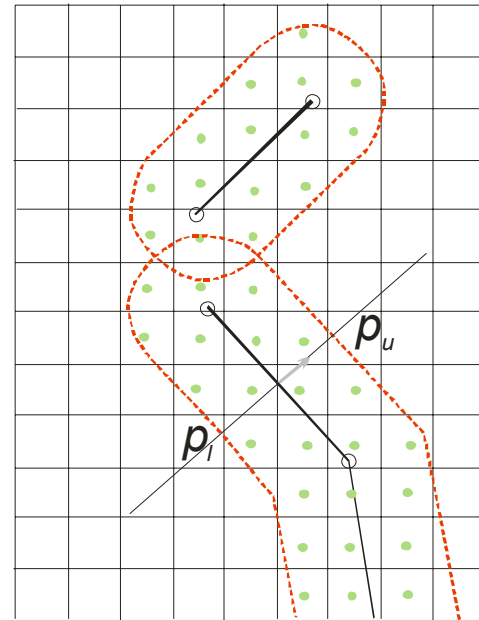
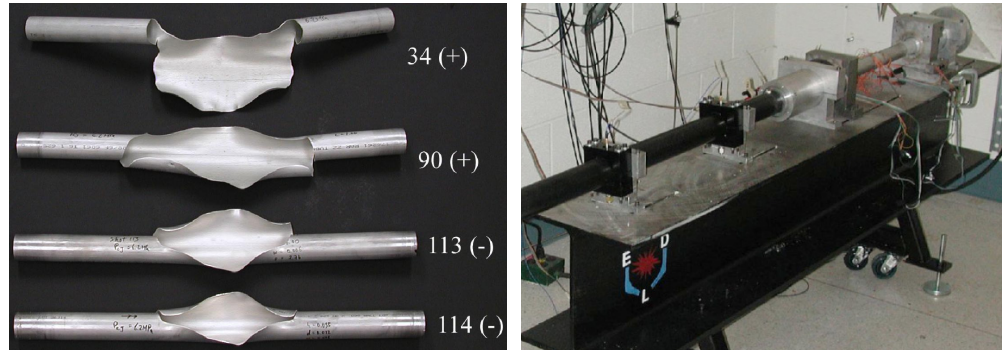
Panel motion – solver verification

- SAMR base mesh 320x64(x2), 2 additional level with factors 2, 2
- Intel 3.4GHz Xeon dual processors connected with Gigabit Ethernet
 - *Beam-FSI*: 12.25h CPU on 3 fluid CPU + 1 solid CPU
 - *FEM-FSI*: 322h CPU on 14 fluid CPU + 2 solid CPU
- Pressure measured at upper boundary, 0.01m before beam



Detonation-driven fracture simulations

- Motivation: Validation for complex fluid-structure interaction problem
- Interaction of detonation, ductile deformation, fracture
- Experiments by T. Chao, J. C. Krok, J. Karnesky, F. Pintgen, J.E. Shepherd
- Thin boundary structures or lower-dimensional shells require “thickening” to apply ghost fluid method
 - Unsigned distance level set function φ
 - Treat cells with $0 < \varphi < d$ as ghost fluid cells (indicated by green dots)
 - Leaving φ unmodified ensures correctness of $\nabla\varphi$
 - Refinement criterion based on φ ensures reliable mesh adaptation
 - Use face normal in shell element to evaluate $\Delta p = p_u - p_l$

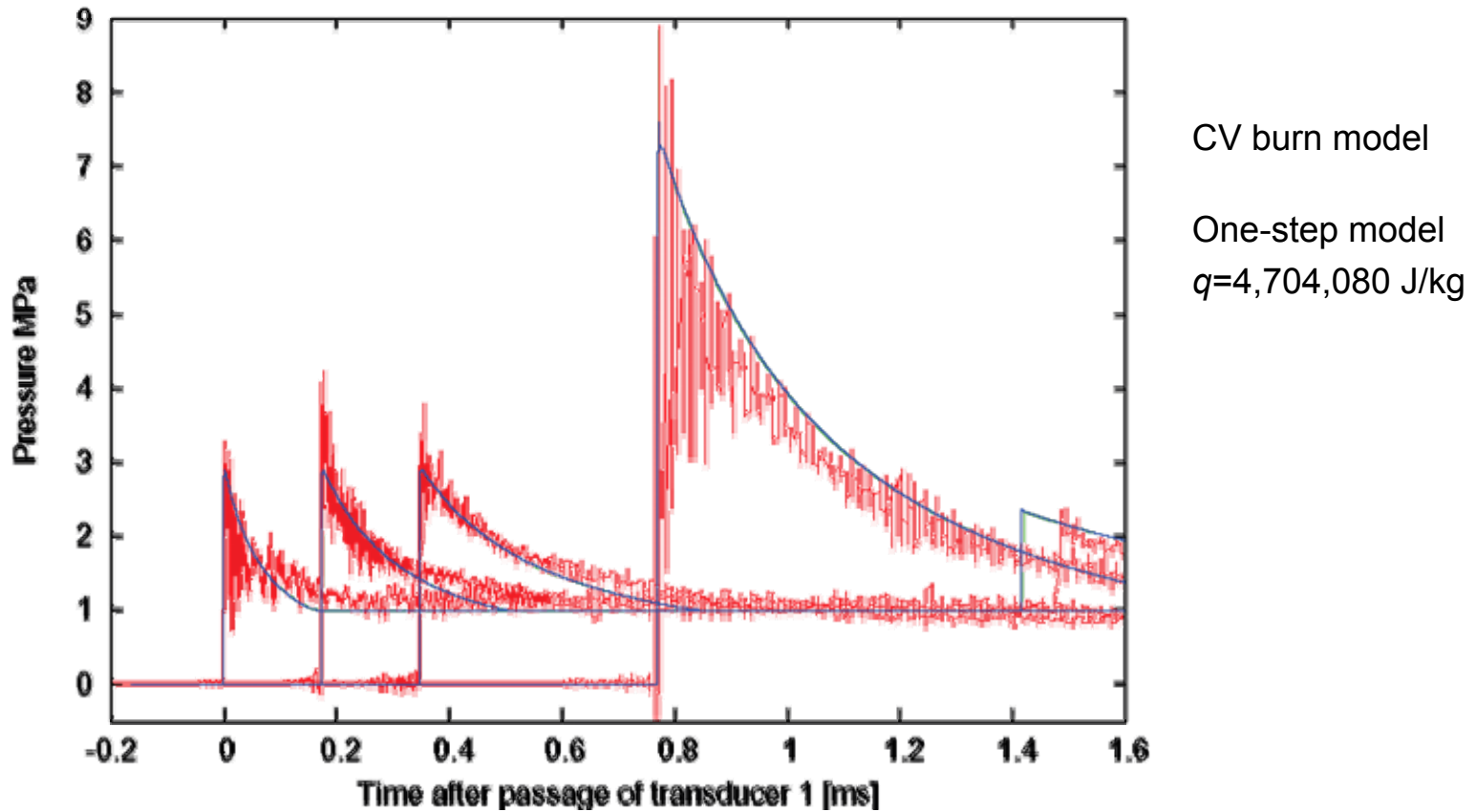


Detonation modeling

- Ethylene-oxyene combustion is impossible to resolve in multiple space-dimensions for this experiment even with one-step reaction model
 - *Unigrid mesh with $10\text{Pts}/\Delta_{1/2} \rightarrow 2 \cdot 10^5 \times (2.4 \cdot 10^4)^2 \approx 1.2 \cdot 10^{14}$ cells in 3D ($\Delta_{1/2} \approx 0.03$ mm, length of detonation tube ≈ 2.1 m)*
- → Modeling of detonation with constant volume burn detonation model by C. Mader (1979)
 - *No explicit source term, but linear enforcing of fully reacted state*
$$Y' := 1 - \frac{V - V_0}{V_{CJ} - V_0}, \quad V = \frac{1}{\rho}, \quad V_0 = \frac{1}{\rho_0}, \quad V_{CJ} = \frac{1}{\rho_{CJ}}$$

if $0 \leq Y' \leq 1$ and $Y > 10^{-8}$
 if $Y < Y'$ and $Y' < 0.9$ then $Y' := 0$
 if $Y' < 0.99$ then $p' := (1 - Y')p_{CJ}$
 else $p' := p$
 $\rho_1 := Y'\rho, \quad \rho_2 := \rho - \rho_1, \quad e := p'/(\gamma - 1) + Y'q$
 - *Parameter q follows uniquely from u_{det}*
 - *Model eliminates von Neumann state completely, but detonation velocity is always correct, independent of the resolution*
- Verification of CV burn model with one-step reaction model
 - *Chosen parameters: $E=25,000$ J/mol, $A=20,000,000$ 1/s*

CV burn model verification and validation: $\gamma=1.24$



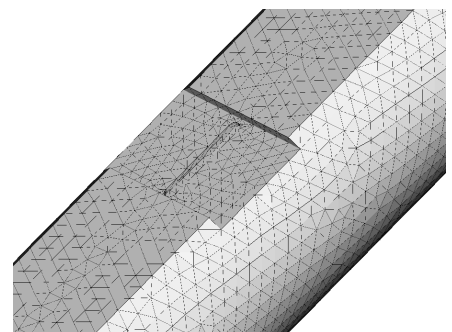
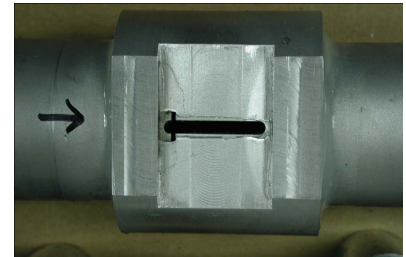
- $p_0 = 100 \text{ kPa}$
- $u_{det} = 2291.7 \text{ m/s}$ (*adjusted to experimentally measured velocity*)
- $\gamma = 1.24$ (*value in CJ point*)

Fluid solver validation - venting event

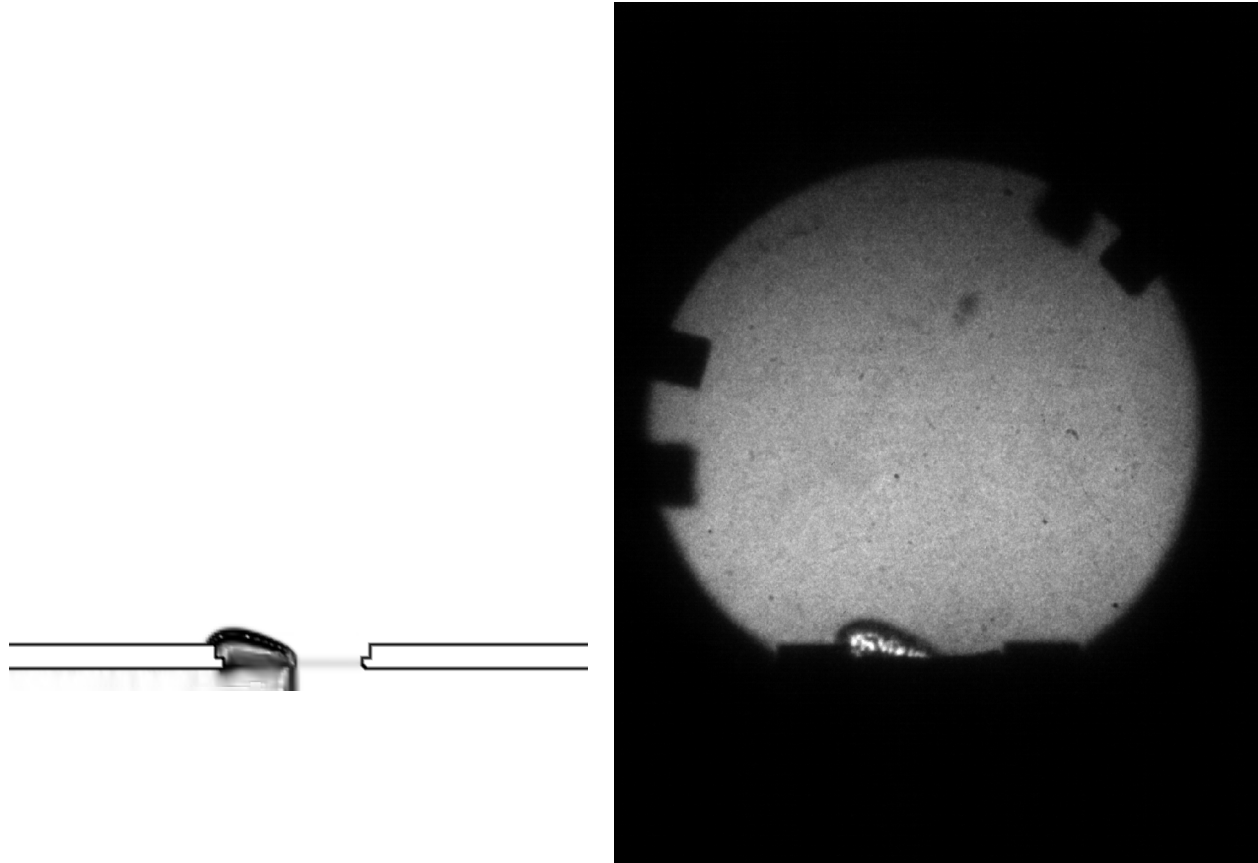
- $\text{C}_2\text{H}_4 + 3 \text{O}_2$ CJ detonation for $p_0 = 100\text{kPa}$ expands into the open through fixed slot

Simulation

- 2nd order upwind finite volume scheme, dimensional splitting
- AMR base level: 108x114x242, 4 additional levels, refinement factor 2,2,2,2
- Approx. $6 \cdot 10^6$ cells used in fluid on average instead of $12.2 \cdot 10^9$ (uniform)
 - *Tube and detonation fully refined*
 - *No refinement for $z < 0$ (to approximate Taylor wave)*
 - *No maximal refinement for $x > 0.1125\text{m}$, $y > 0.1125\text{m}$, $z < 0.37\text{m}$, $z > 0.52\text{m}$*
- Thickening of 2d mesh: 0.445mm on both sides additional to real thickness of both sides 0.445mm
- Solid mesh: 28279 nodes, 56562 elements
- 16 nodes 2.2 GHz AMD Opteron quad processor, ~3300h CPU to $t=3$ ms

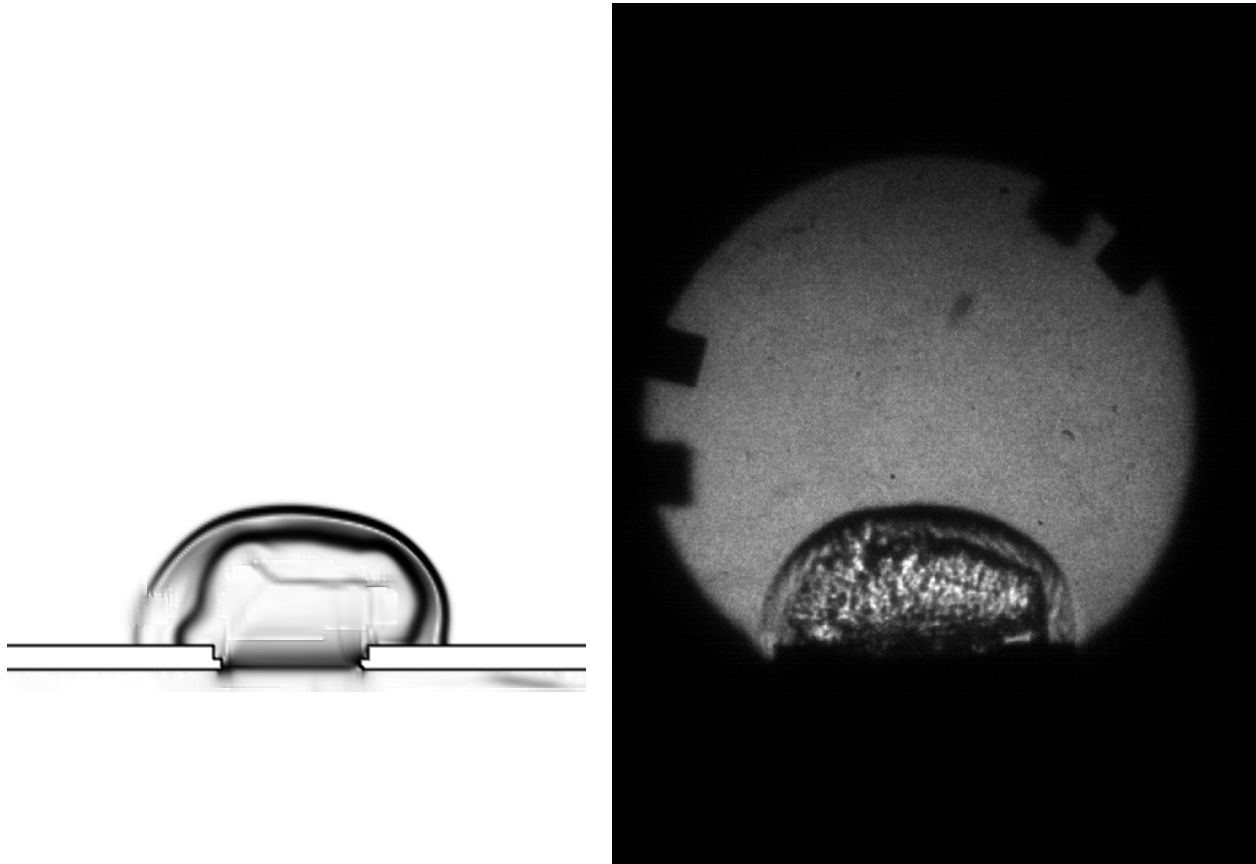


Venting event – computational results



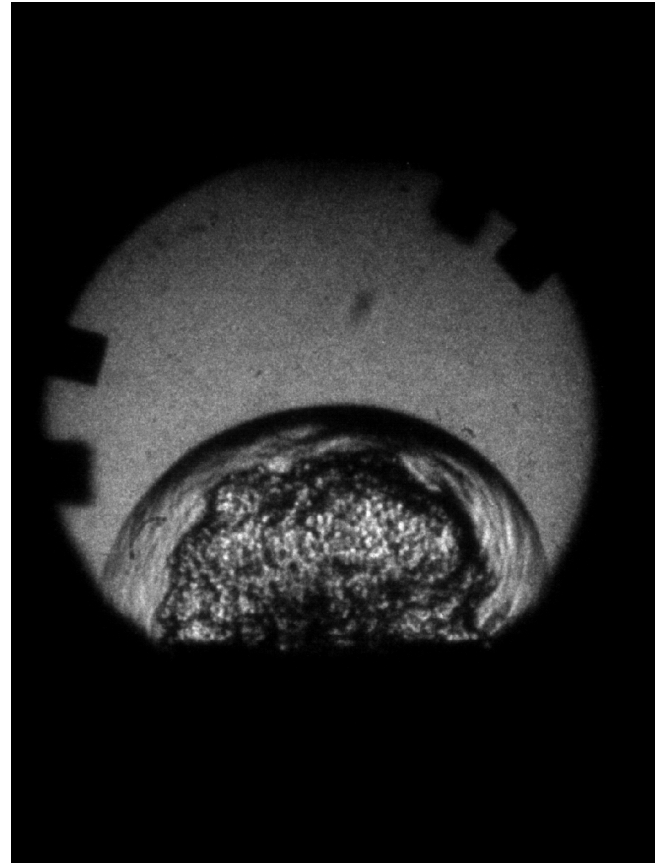
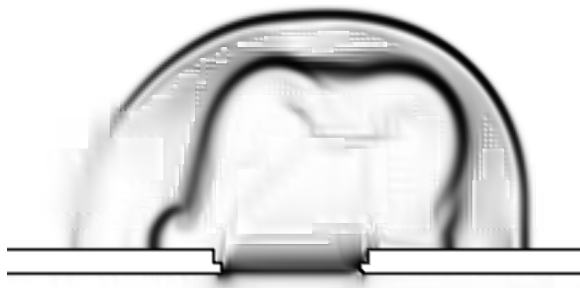
Comparison of simulated and experimental results at $t=0 \mu\text{s}$

Venting event – computational results



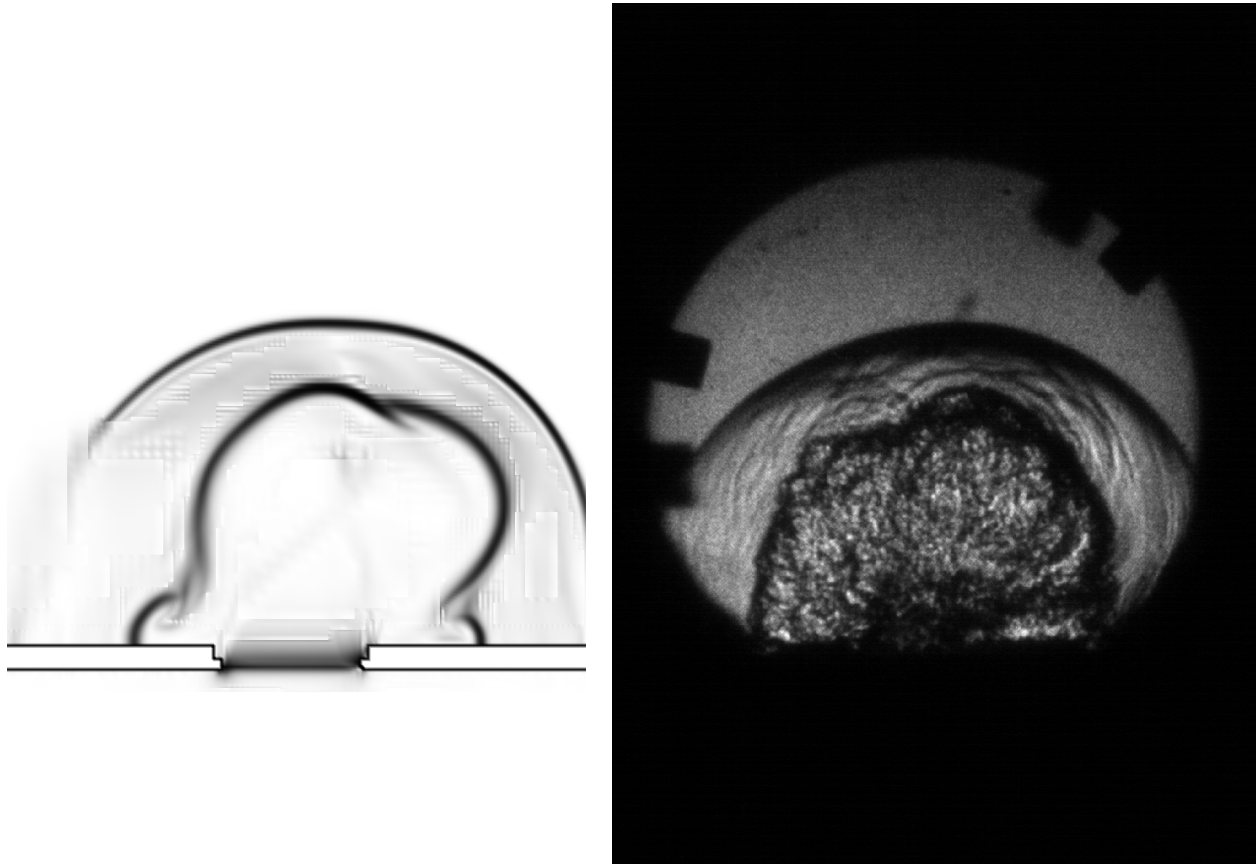
Comparison of simulated and experimental results at $t = 30 \mu\text{s}$

Venting event – computational results



Comparison of simulated and experimental results at $t=60 \mu\text{s}$

Venting event – computational results



Comparison of simulated and experimental results at $t = 90 \mu\text{s}$

Coupled simulations in elastic regime – vibrational coupling

- C₂ H₄+3 O₂ CJ detonation for $p_0=80\text{kPa}$ induces tube vibrations
- Motivation:
 - Verify dynamically adaptive fluid-structure interaction method for full configuration
 - Validate material model in elastic regime

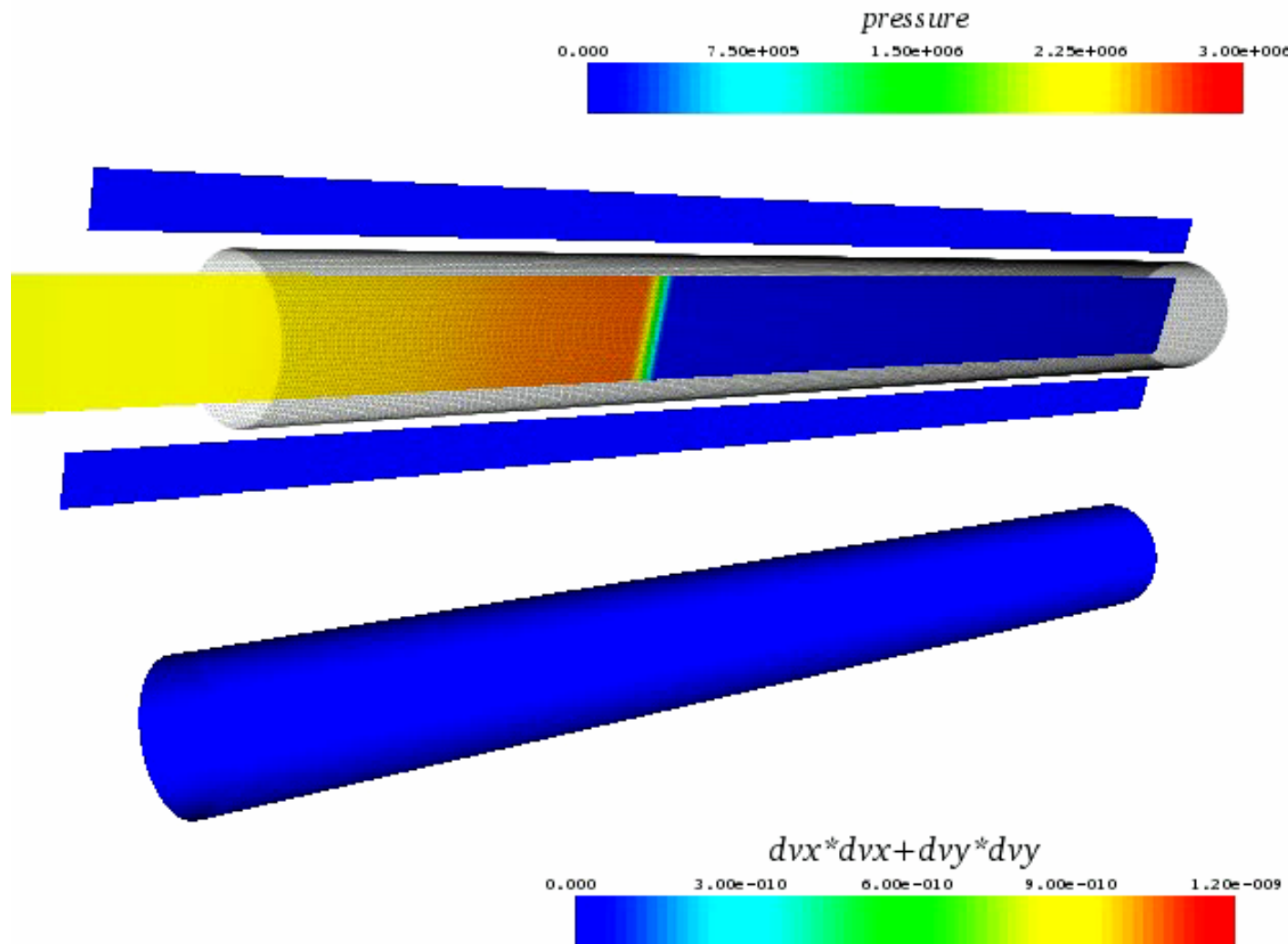
Fluid

- Constant volume burn model
- AMR base level: 20x20x406, 2 additional levels, factors 2,2

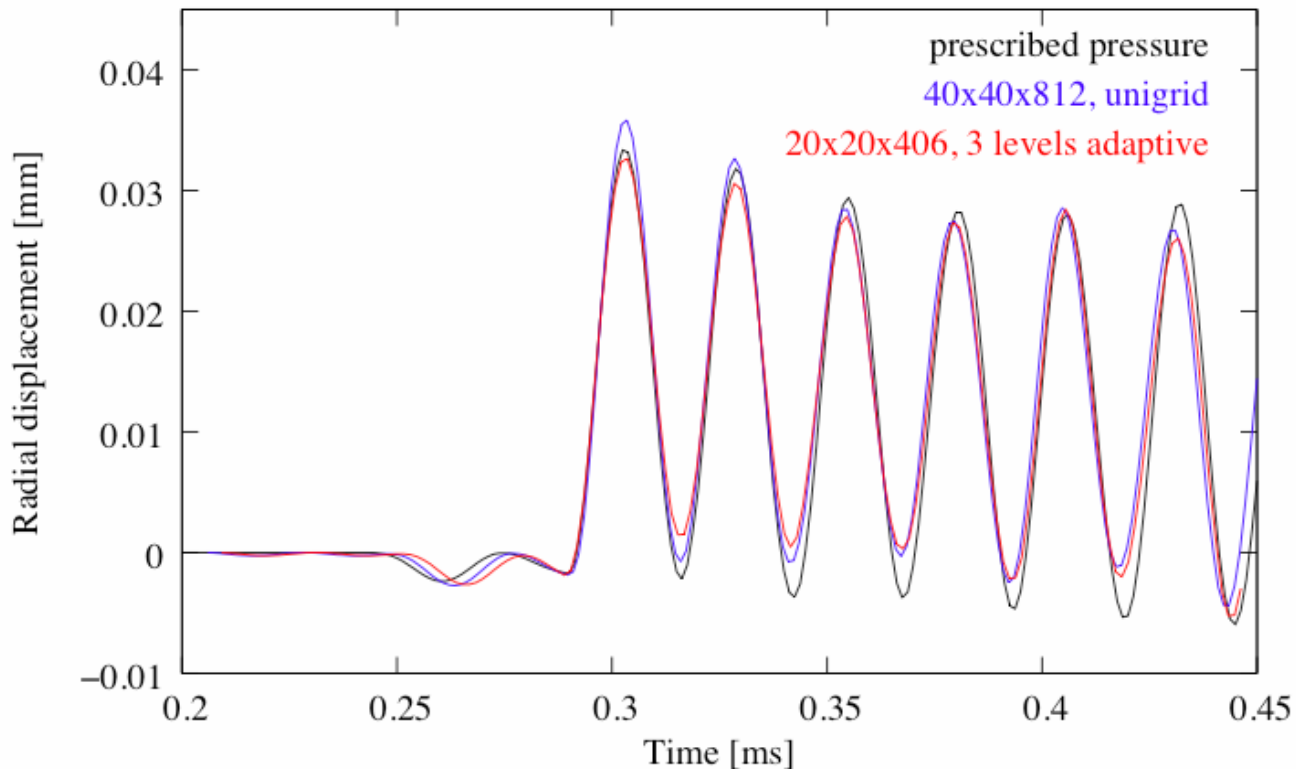
Solid

- Aluminum, J2 plasticity with hardening, rate sensitivity, and thermal softening
- Mesh: 84288 elements
- 25+7 Itanium-2 processors, ~384h CPU

Coupled simulations in elastic regime – vibrational coupling



Coupled simulations in elastic regime



- Convergence for resolution increase from fluid mesh adaptation
- Good agreement with CV burn model simulations with prescribed pressure profile derived from Taylor-Zeldovich model

$$p(x, t) = \begin{cases} 0, & 0 < t < t_{cj} \\ (p_{cj} - p_{tail})e^{(t_{cj}-t)/T} + p_{tail}, & t_{cj} < t < \infty \end{cases}$$

Fluid-structure interaction validation – tube with flaps

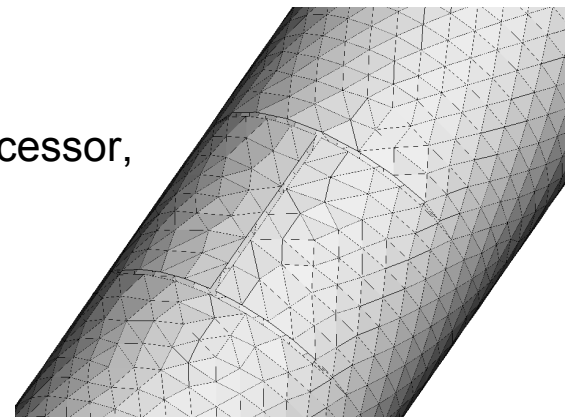
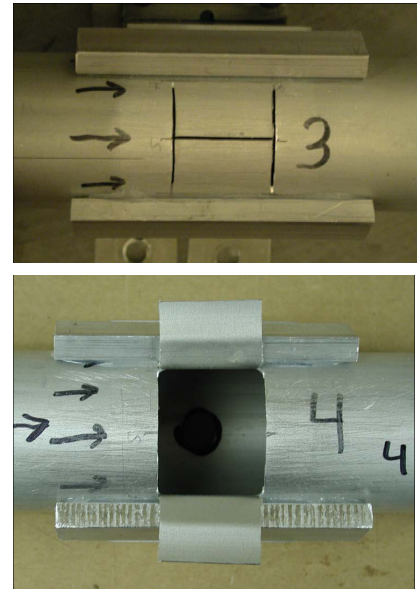
- $\text{C}_2\text{H}_4 + 3 \text{O}_2$ CJ detonation for $p_0 = 100\text{kPa}$ drives plastic opening of pre-cut flaps
- Motivation:
 - Validate fluid-structure interaction method
 - Validate material model in plastic regime

Fluid

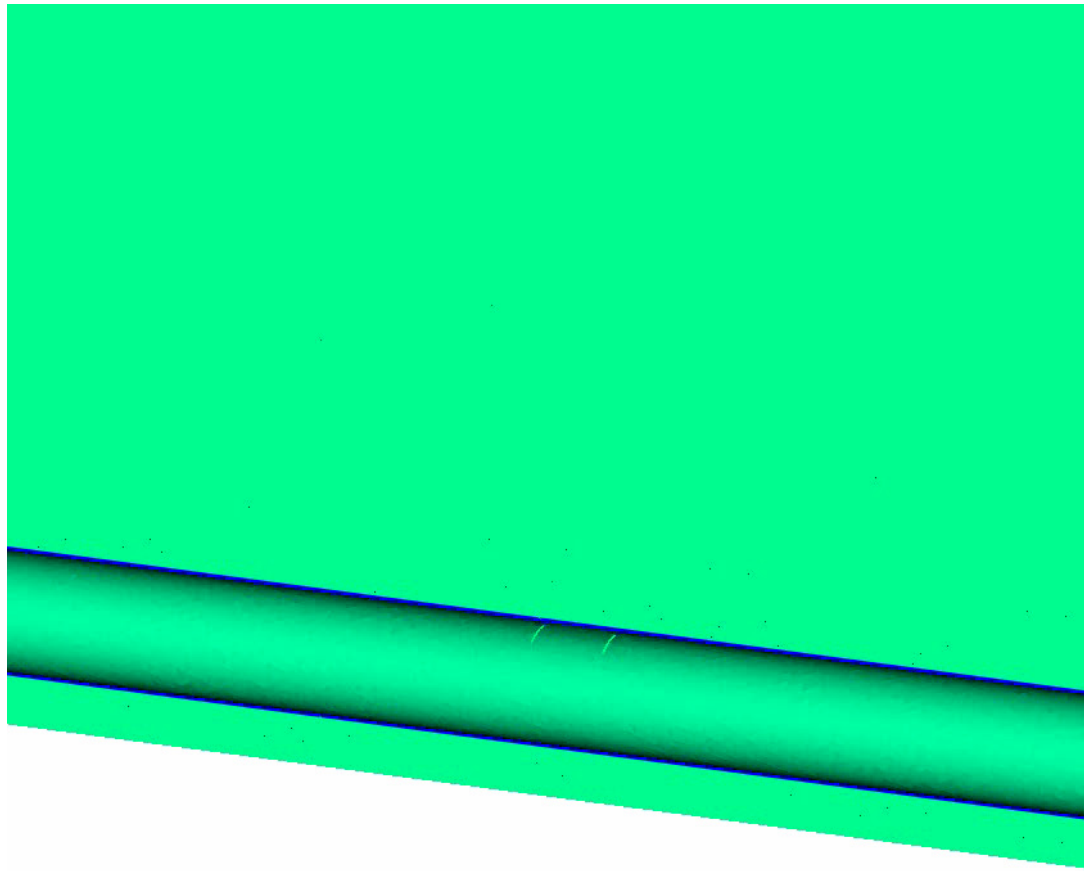
- Constant volume burn model
- AMR base level: 104x80x242, 3 additional levels, factors 2,2,4
- Approx. $4 \cdot 10^7$ cells instead of $7.9 \cdot 10^9$ cells (uniform)
- Tube and detonation fully refined
- Thickening of 2d mesh: 0.81mm on both sides (real thickness on both sides 0.445mm)

Solid

- Aluminum, J2 plasticity with hardening, rate sensitivity, and thermal softening
- Mesh: 8577 nodes, 17056 elements
- 16+2 nodes 2.2 GHz AMD Opteron quad processor, ~ 4320h CPU to $t=450 \mu\text{s}$



Tube with flaps – computational results

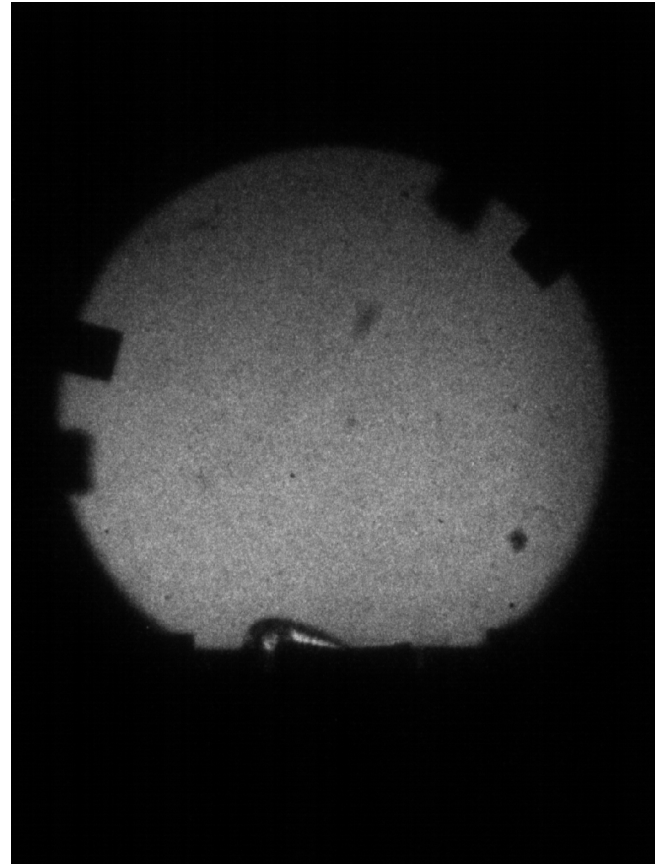


Fluid density and displacement in y-direction in solid

Tube with flaps – computational results



Simulated results at $t=2 \mu\text{s}$

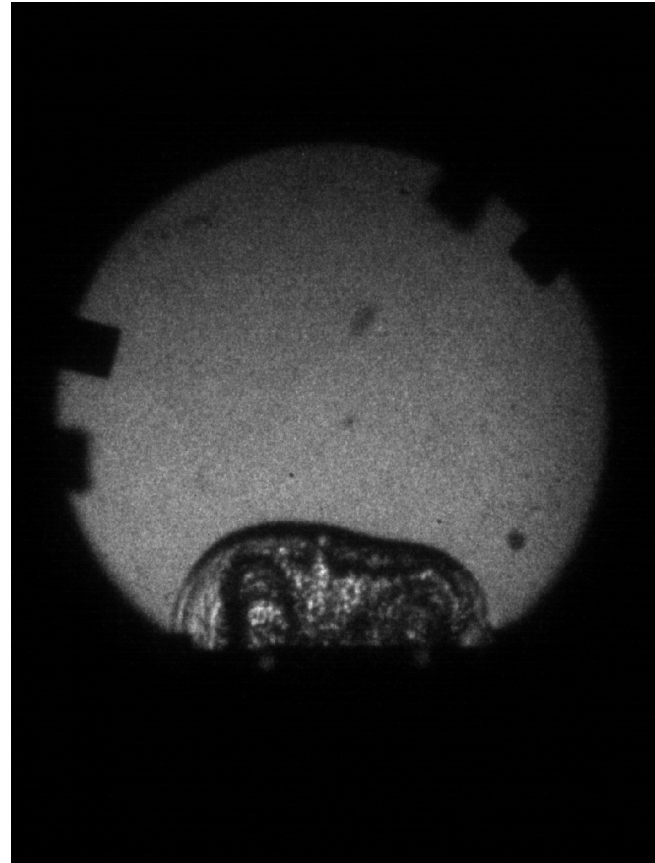


Experimental results at $t=0 \mu\text{s}$

Tube with flaps – computational results

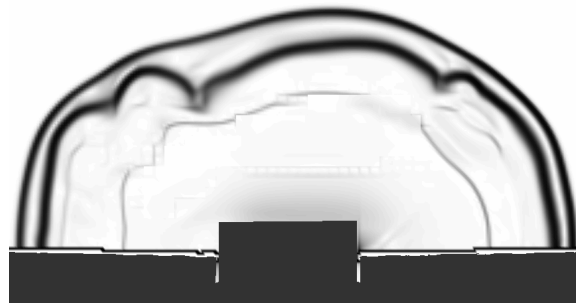


Simulated results at $t=32 \mu\text{s}$

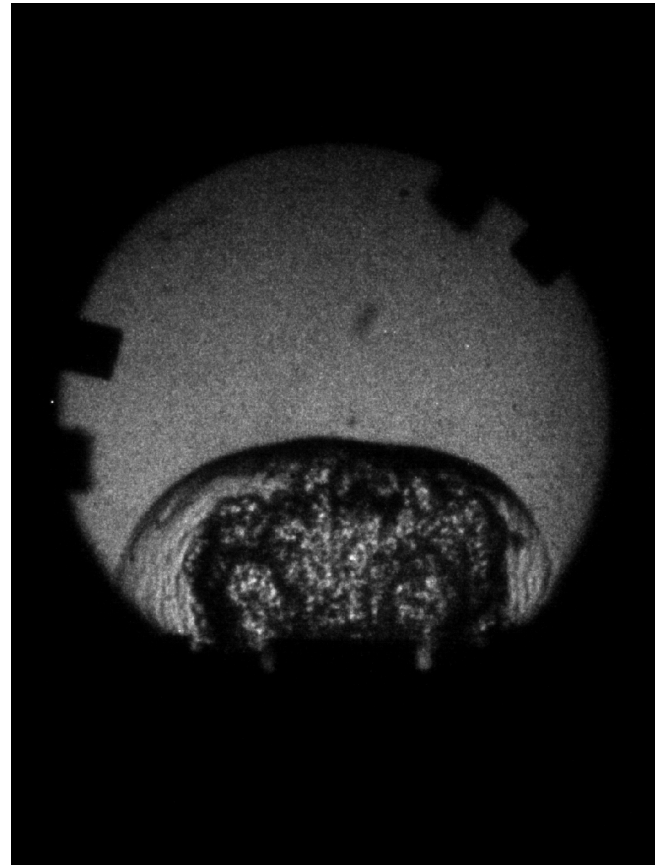


Experimental results at $t=30 \mu\text{s}$

Tube with flaps – computational results

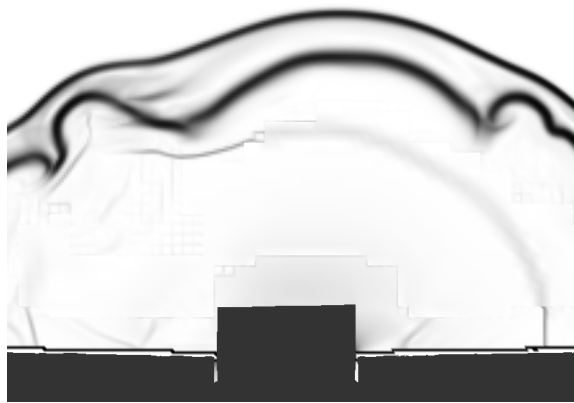


Simulated results at $t=62 \mu\text{s}$

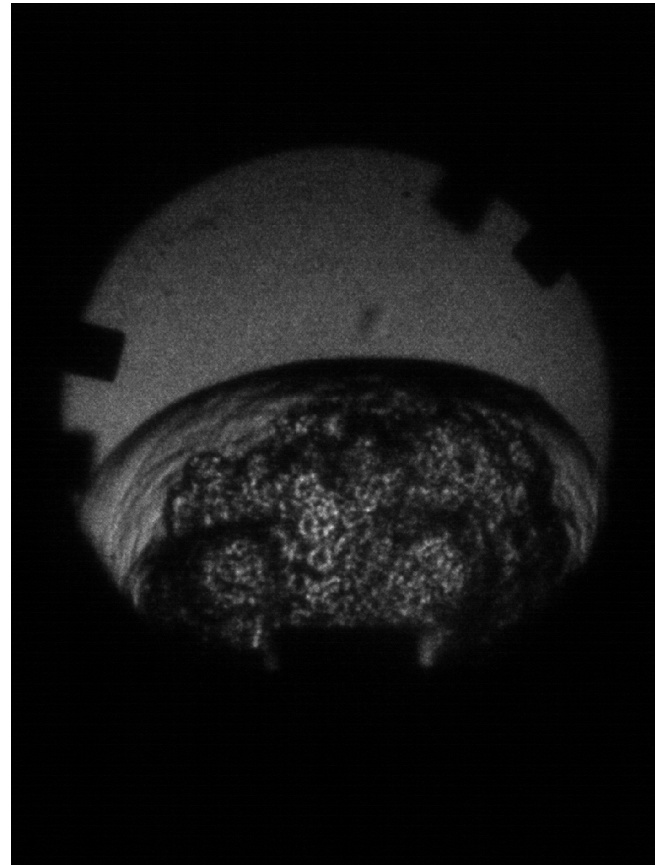


Experimental results at $t=60 \mu\text{s}$

Tube with flaps – computational results

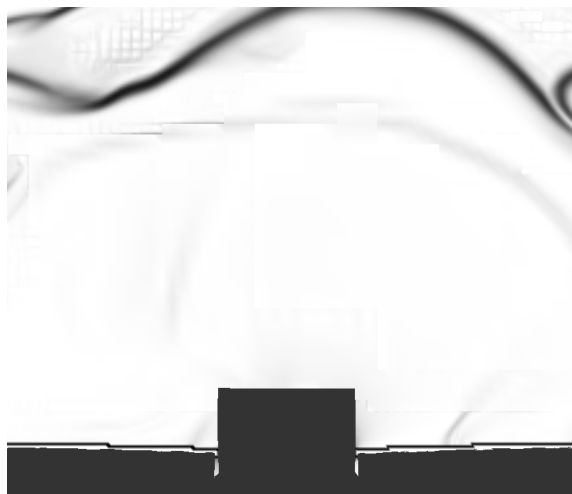


Simulated results at $t=92 \mu\text{s}$

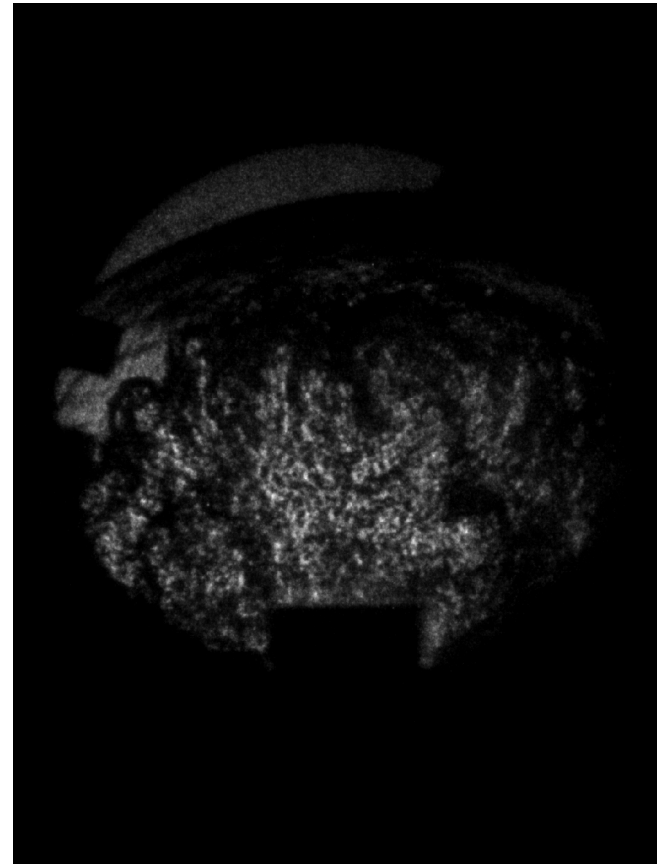


Experimental results at $t=90 \mu\text{s}$

Tube with flaps – computational results



Simulated results at $t=152 \mu\text{s}$

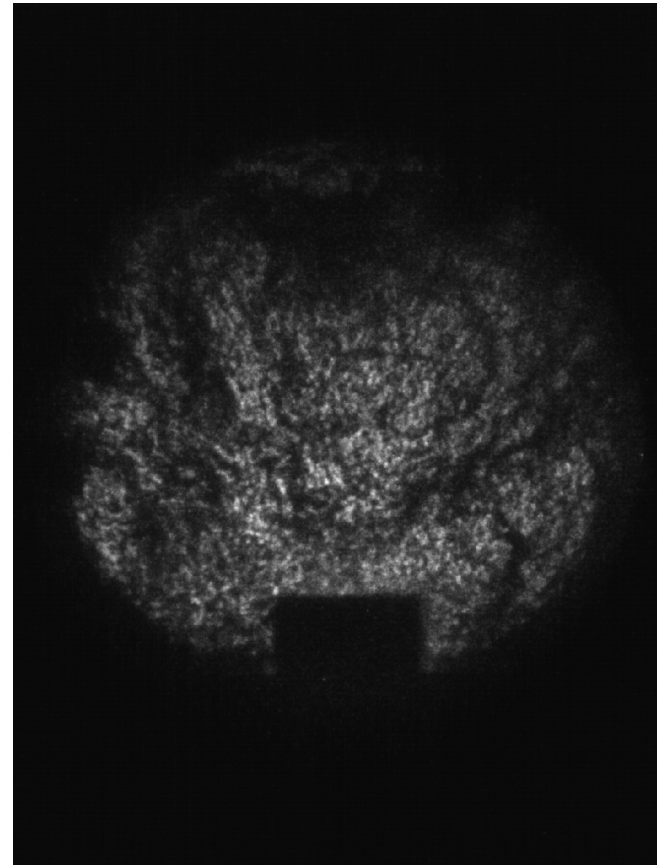


Experimental results at $t=150 \mu\text{s}$

Tube with flaps – computational results

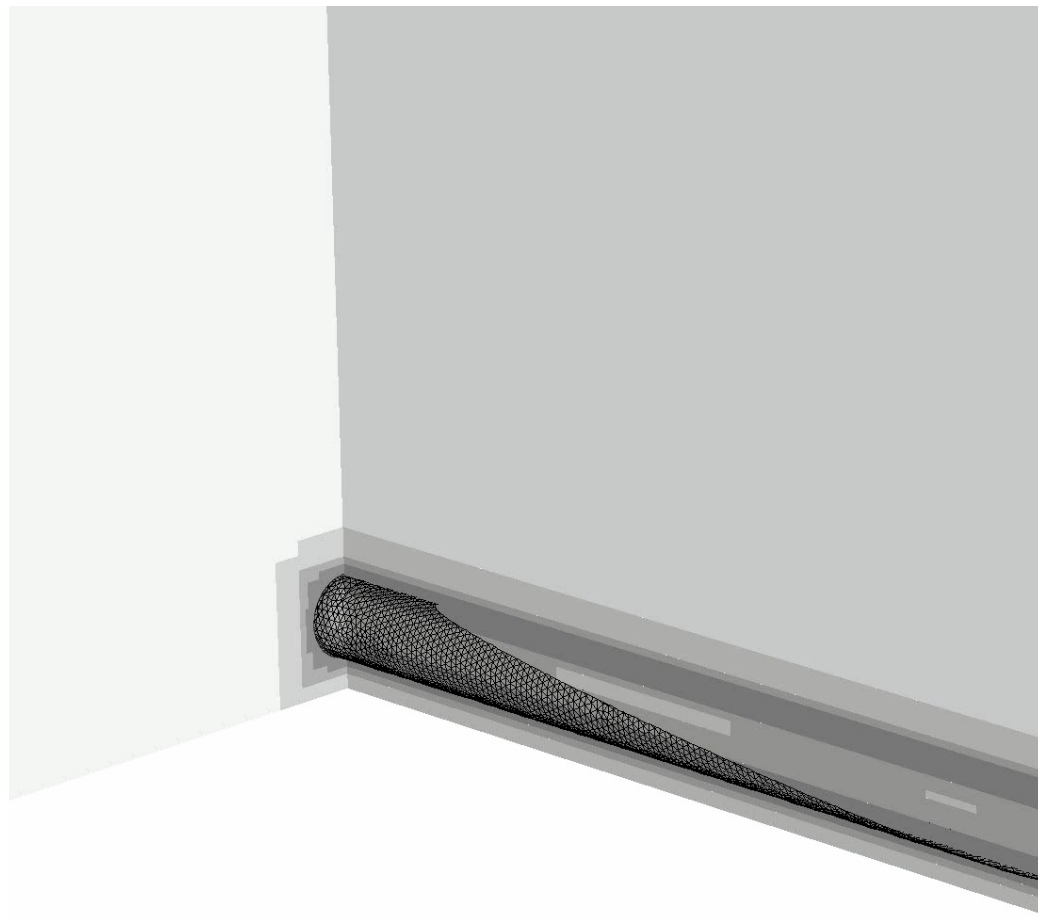


Simulated results at $t=212 \mu\text{s}$



Experimental results at $t=210 \mu\text{s}$

Tube with flaps – fluid mesh adaptation



Schlieren plot of fluid density on refinement levels

Coupled fracture simulation

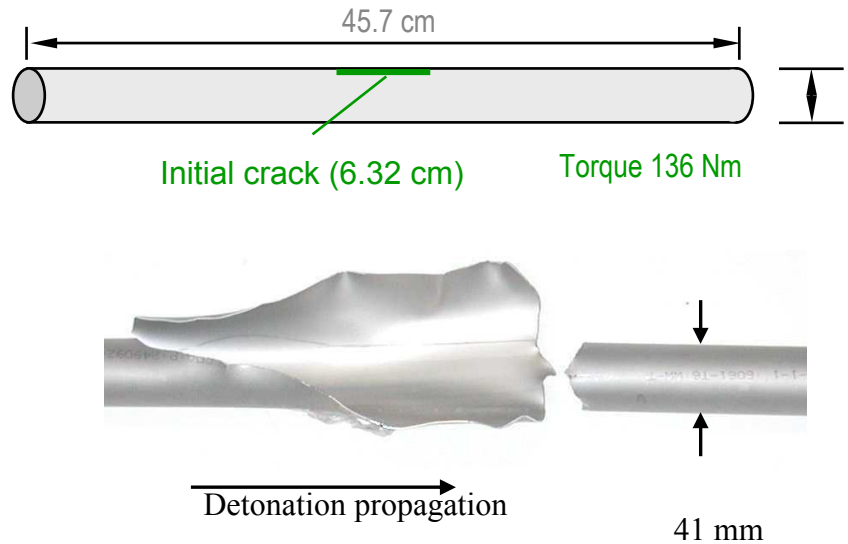
- C₂H₄+3 O₂ CJ detonation for $p_0=180\text{kPa}$ drives tube fracture
- Motivation: Full configuration

Fluid

- Constant volume burn model
- 40x40x725 cells unigrid

Solid

- Aluminum, J2 plasticity with hardening, rate sensitivity, and thermal softening
- Material model for cohesive interface: Linearly decreasing envelope
- Mesh: 206,208 nodes
- 27 nodes Pentium 4-dual-processor with 33 shell and 21 fluid processors
- Ca. 972h CPU



Coupled fracture simulation

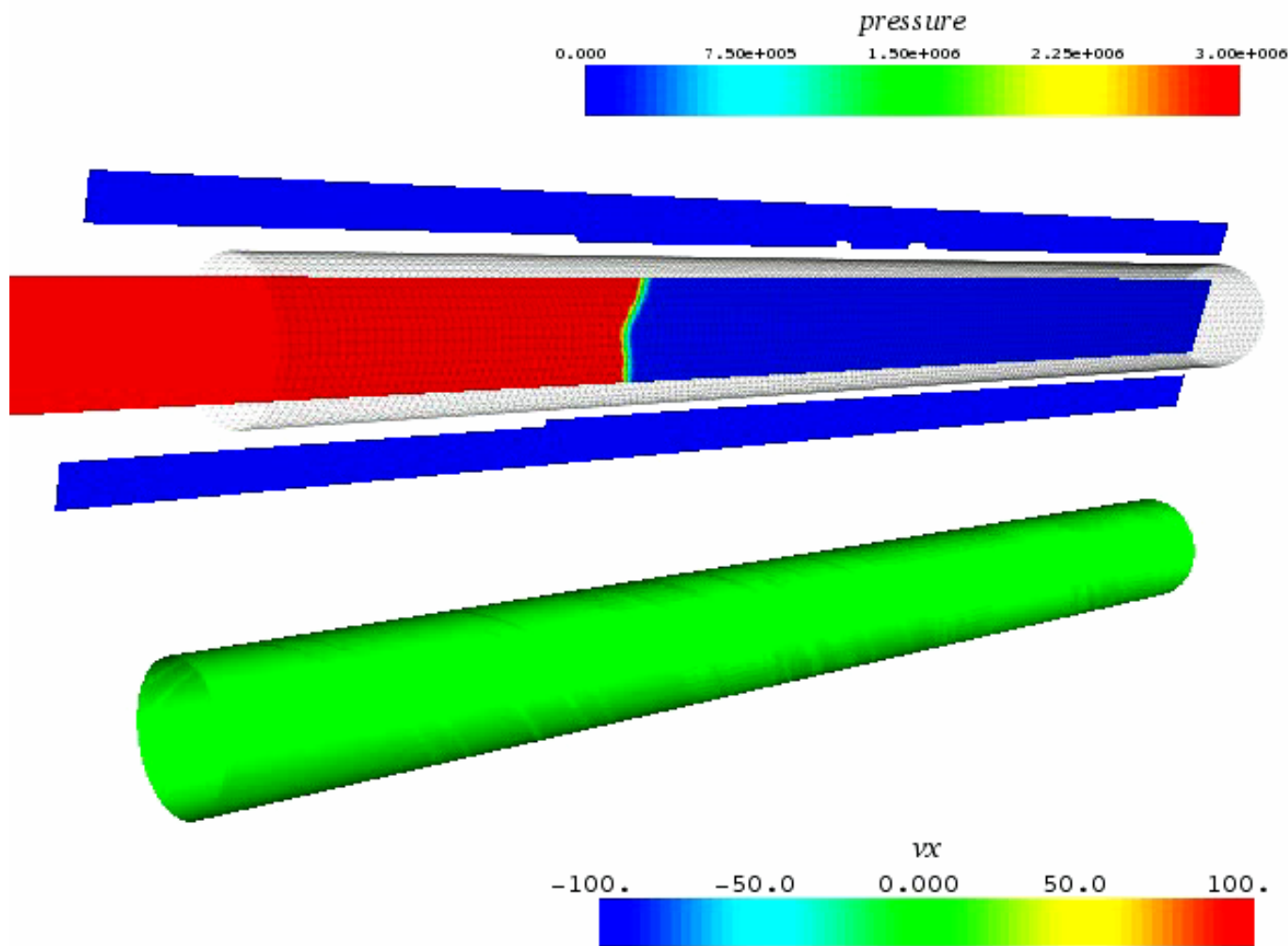
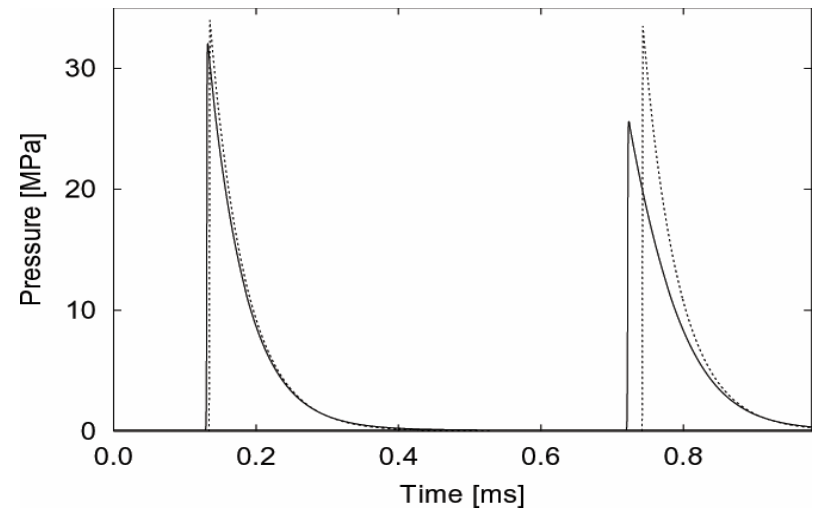
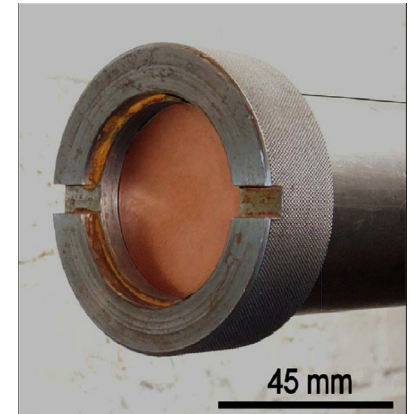
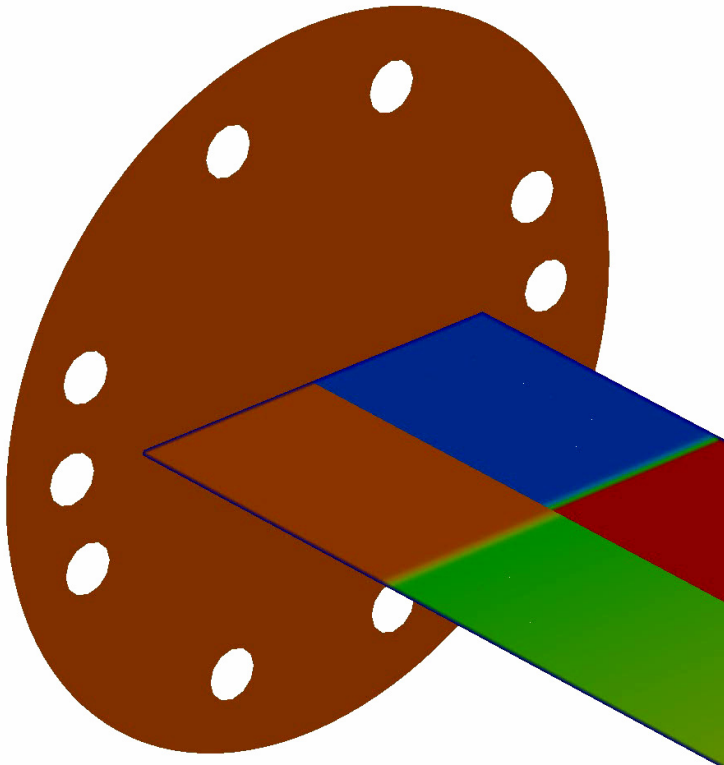


Plate deformation from water hammer

- 3d simulation of plastic deformation of thin copper plate attached to the end of a pipe due to water hammer
- Experiment by V.S. Deshpande et al. (U Cambridge)
- Strong over-pressure wave in water is induced by rapid piston motion at end of tube
- Modeling of water with stiffened gas equation of state with $\gamma=7.415$, $p_\infty=296.2$ MPa
- Realistic pressure loading in simulations created by solving equation of motion for piston
- Left: comparison of simulated pressure wave compared to analytically derived traveling wave solution (dotted) for initial pressure $p_0=34$ MPa

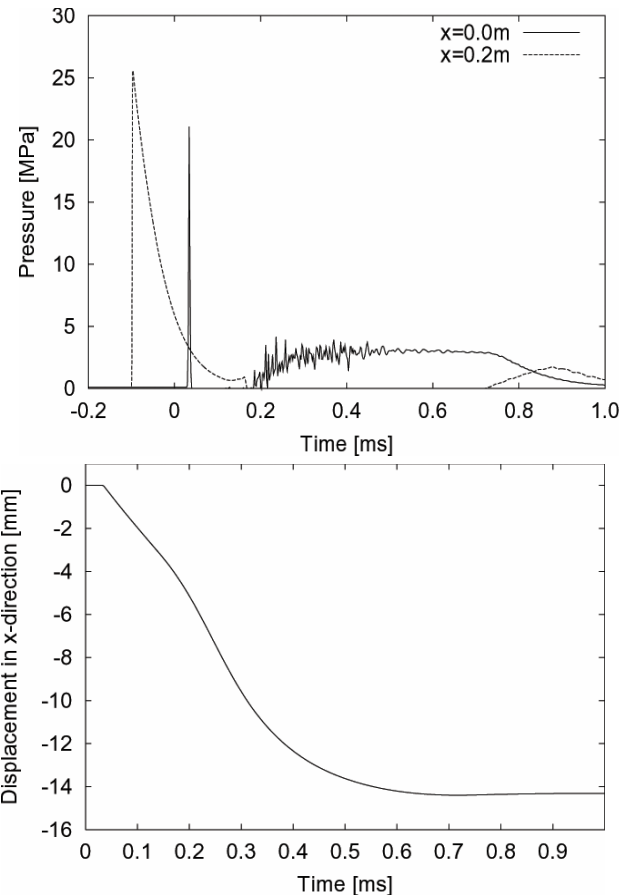


Plastic deformation

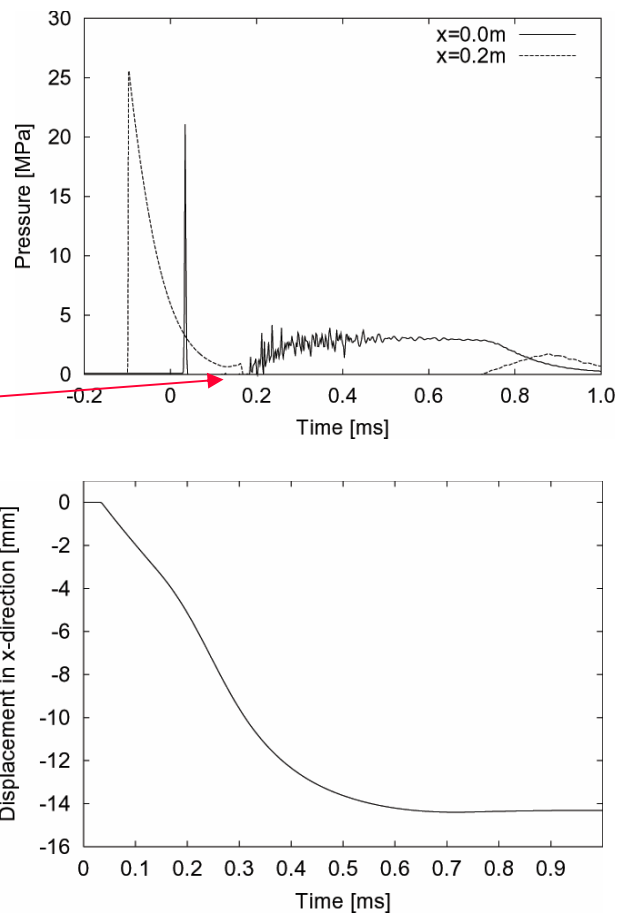
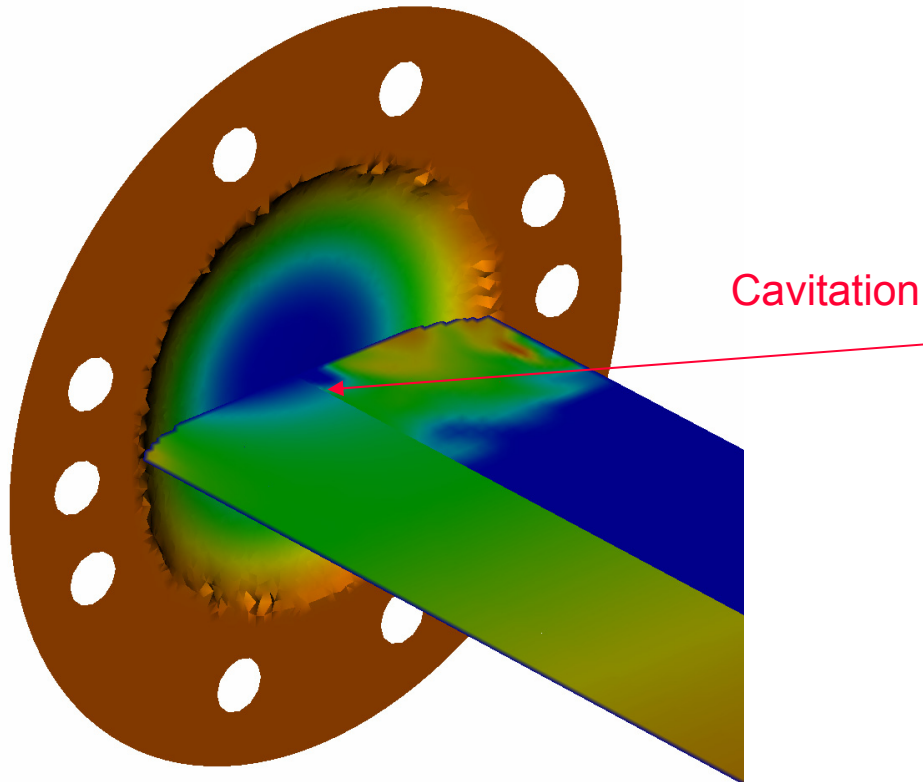


Color of plate and lower half of plane shows the normal velocity

- $p_0 = 34 \text{ MPa}$
- 8 nodes 3.4 GHz Intel Xeon dual processor, $\sim 130\text{h CPU}$

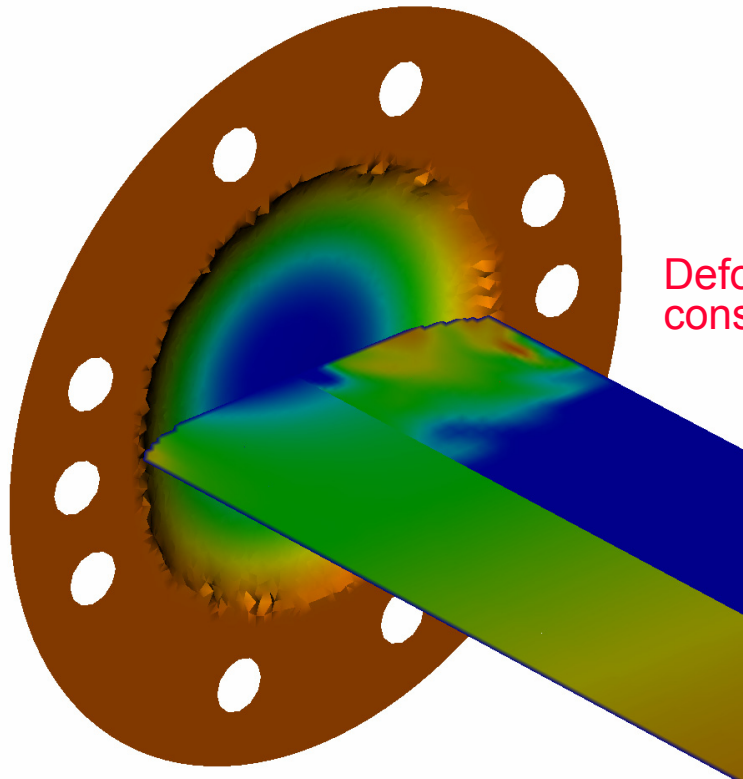


Plastic deformation

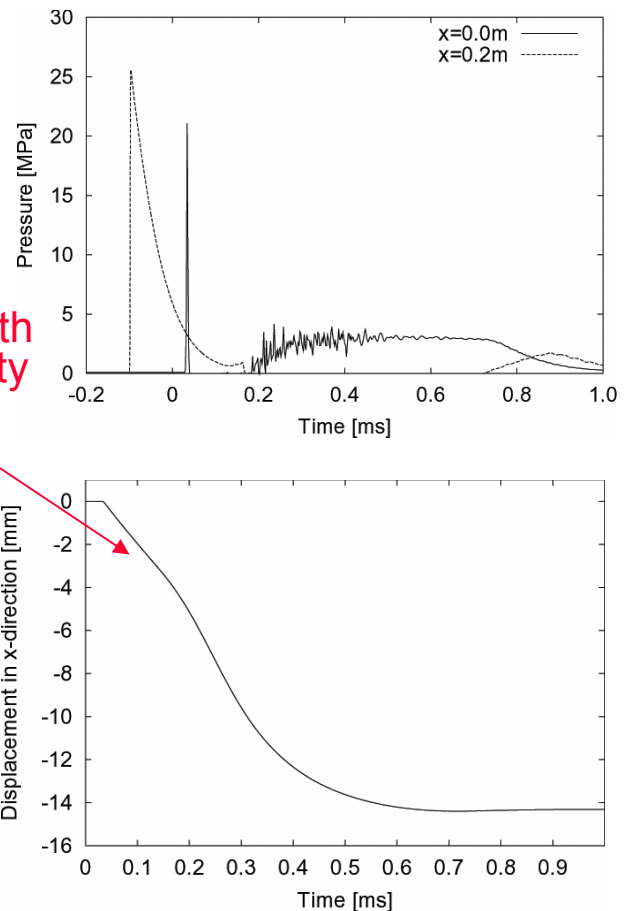


- $p_0 = 34 \text{ MPa}$
- 8 nodes 3.4 GHz Intel Xeon dual processor, $\sim 130\text{h CPU}$

Plastic deformation

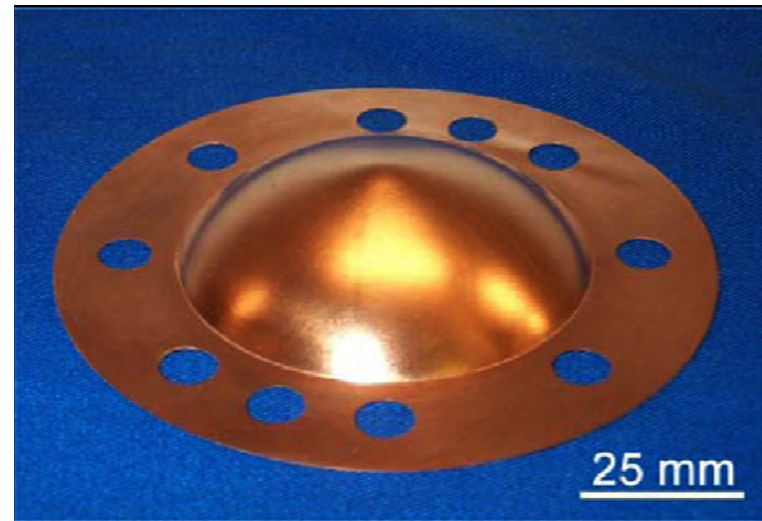
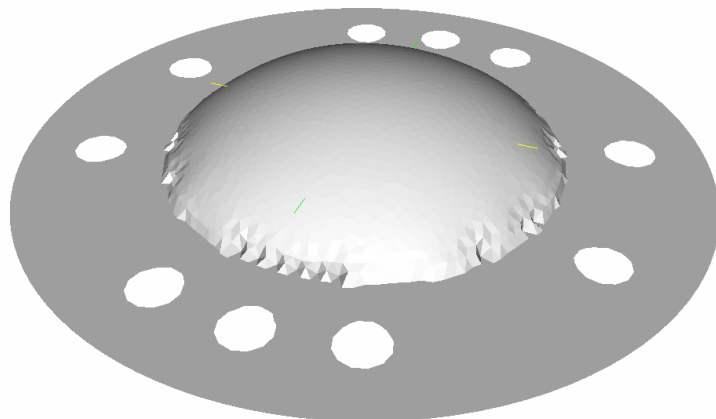


Deformation with
constant velocity



- $p_0 = 34 \text{ MPa}$
- 8 nodes 3.4 GHz Intel Xeon dual processor, $\sim 130\text{h CPU}$

Plate deformation



Comparison of plate at end of simulation and experiment.

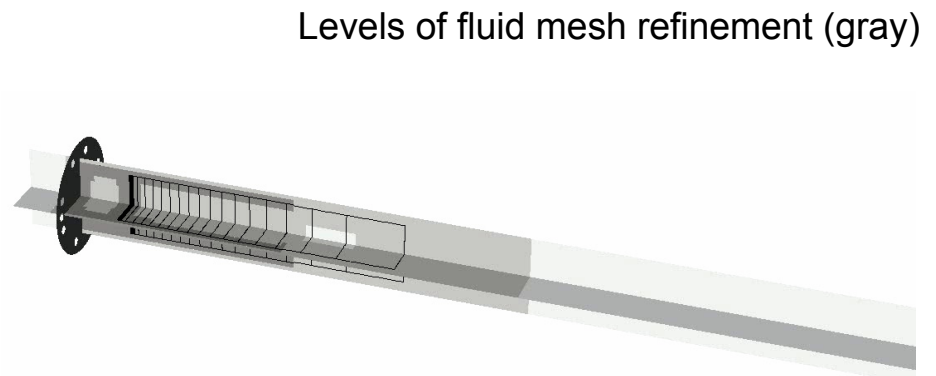
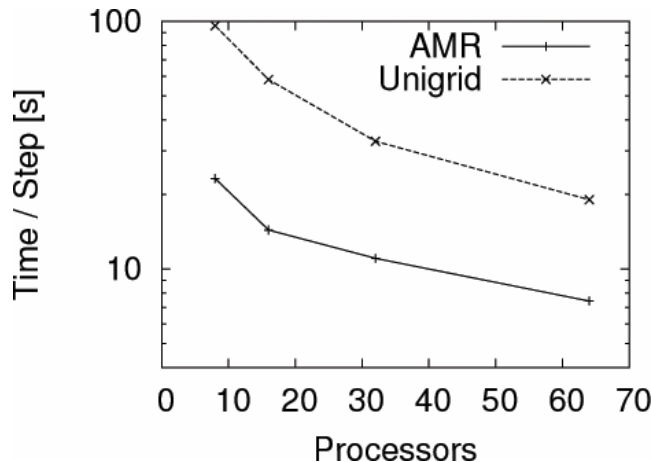
Simulation details

Fluid

- Multi-dimensional 2nd order upwind finite volume scheme, negative pressures from cavitation eliminated by energy correction
- AMR base level: 350x20x20, 2 additional levels, refinement factor 2,2
- Approx. $1.2 \cdot 10^6$ cells used in fluid on average instead of $9 \cdot 10^6$ (uniform)

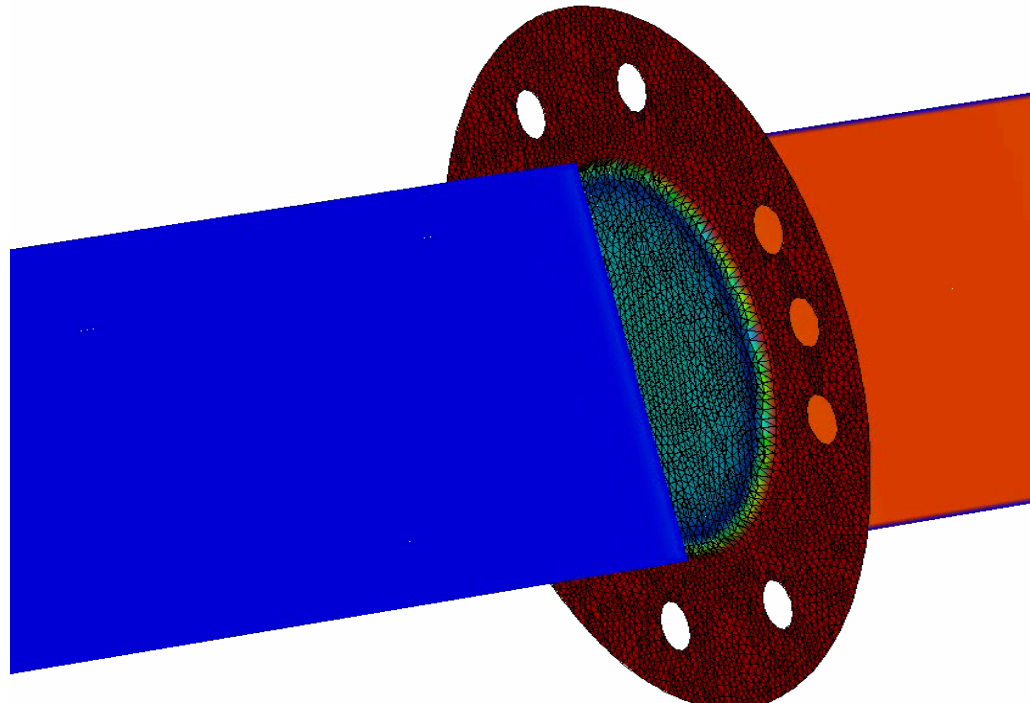
Solid

- Copper plate of 0.25mm, J2 plasticity model with hardening, rate sensitivity, and thermal softening
- Solid mesh: 4675 nodes, 8896 elements



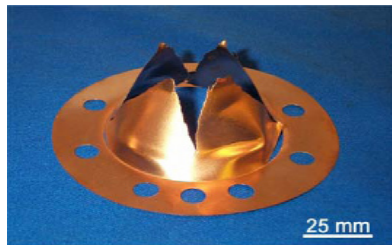
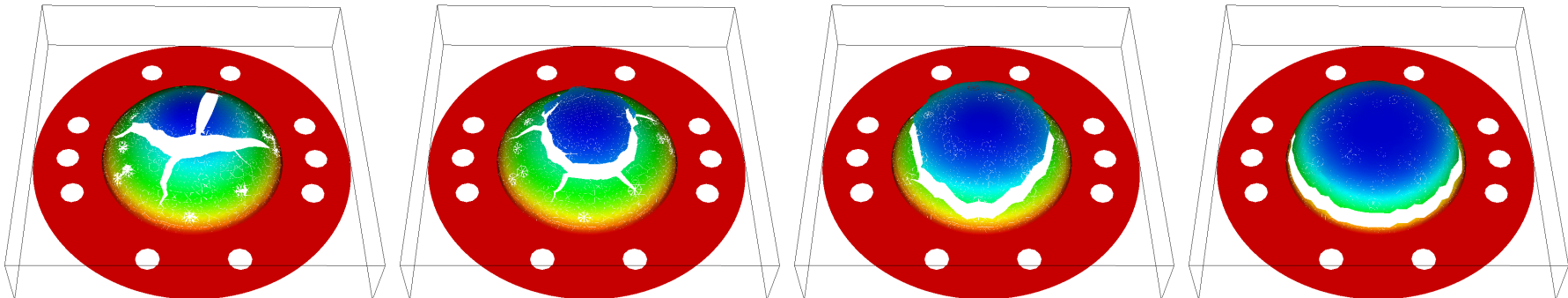
Levels of fluid mesh refinement (gray)

Plate fracture



- Two-component solver with stiffened gas EOS for water and ideal gas EOS for air
- Material model for cohesive interface: linear decreasing envelope
- 4+4 nodes 3.4 GHz Intel Xeon dual processor, ~550h CPU

Comparison of fracture pattern



$p_0=64 \text{ MPa}$



$p_0=88 \text{ MPa}$



$p_0=130 \text{ MPa}$



$p_0=173 \text{ MPa}$

- Variation of loading conditions
- Computations stopped at different times, when fracture pattern were clearly established

Conclusions

- Developed Cartesian Eulerian fluid solver framework that allows easy coupling to Lagrangian solid mechanics solver
- Focus is currently on time-explicit schemes and weak coupling
- Generic ghost fluid implementation allows consideration of moving embedded boundaries in any structured finite volume method
- Boundaries can be described directly through level set functions or arbitrary triangulated surface meshes
- Structured mesh adaptation ensures accuracy
- Several Interfaces to volumetric research finite element solvers already implemented, e.g. LLNL Dyna3d
- Developed efficient transformation algorithm for on-the-fly level set evaluation
- All components parallelized with MPI for distributed memory machines

Virtual Test Facility software

- Make majority of software available to open source community
 - *Release fully functional solvers with large number of single-solver applications plus several fully functional FSI applications*
 - *Include solver and FSI unit tests plus reference results to allow users to verify software integrity*
- Language: object-oriented C++ with components in C, F77, F90
- autoconf / automake environment with support for typical parallel high-performance systems
- Webpage: <http://www.cacr.caltech.edu/asc>
 - *Installation, configuration, examples*
 - *Scientific and technical papers*
 - *Archival of key simulation and experimental results*
 - *Source code documentation*
 - *Downloadable software (not yet) with example simulations*

